JOURNAL OF GEOPHYSICAL RESEARCH, VOL. 104, NO. D11, PAGES 13,791–13,823, JUNE 20, 1999

Global concentrations of tropospheric sulfate, nitrate, and ammonium aerosol simulated in a general circulation model

Peter J. Adams and John H. Seinfeld
Department of Chemical Engineering, California Institute of Technology, Pasadena

Dorothy M. Koch
National Aeronautics and Space Administration Goddard Institute for Space Studies, New York

Abstract. Global sulfate aerosol composition is simulated online in the Goddard Institute for Space Studies general circulation model II′ (GISS GCM II-prime). Four sulfur species, hydrogen peroxide, gas phase ammonia, and particulate ammonium are the prognostic tracer species, the emissions, transport, and deposition of which are explicitly simulated. Nitric acid fields are prescribed based on a global chemical transport model. An online thermodynamic equilibrium calculation determines the partitioning of ammonia and nitrate between gas and aerosol phases, and the quantity of aerosol water based on the temperature, relative humidity, and sulfate concentration in each GCM grid cell. The total global burden of sulfate, nitrate, ammonium, and aerosol water is 7.5 Tg and is most sensitive to changes in sulfur emissions. Tropospheric lifetimes for ammonium and ammonia are 4.2 and 0.9 days, respectively; the tropospheric ammonium burden is 0.30 Tg N, compared with 0.14 Tg N for ammonia. Simulated ammonium concentrations are generally within a factor of 2 of observations. Subgrid variability in measured concentrations hinders comparison of observations to predictions. Ammonium nitrate aerosol plays an important role in determining total aerosol mass in polluted continental areas. In the upper troposphere and near the poles, cold temperatures allow unneutralized nitric acid to condense into the aerosol phase. Acidic aerosol species tend to be neutralized by ammonia to a greater degree over continents than over oceans. The aerosol is most basic and gas phase ammonia concentrations are highest over India. Water uptake per mole of sulfate aerosol varies by two orders of magnitude because of changes in relative humidity and aerosol composition. Spatial variations in aerosol composition and water uptake have implications for direct and indirect aerosol radiative forcing.

1. Introduction

In recent years, substantial progress has been made towards understanding how airborne aerosols, especially sulfate, influence the Earth's climate and atmospheric chemistry [*Intergovernmental Panel on Climate Change (IPCC)*, 1996; *National Research Council*, 1996]. Sulfate aerosols directly perturb the atmospheric radiation balance by scattering sunlight back into space. Sulfate particles are also an important source of cloud condensation nuclei (CCN), and the number and composition of sulfate particles help to determine resulting cloud properties. In such a way, changes in aerosol sulfate may indirectly perturb the atmospheric radiation balance by influencing the optical properties of clouds. Determining the magnitude and geographical distribution of climate forcing from sulfate aerosols is one of the key outstanding issues in assessing anthropogenic influence on climate. The aerosol sulfate anion is just one of many forms of atmospheric sulfur, including sulfur dioxide (SO_2), dimethyl sulfide (DMS), methanesulfonic acid (MSA), hydrogen sulfide (H_2S), carbon disulfide (CS_2), carbonyl sulfide (COS), dimethylsulfoxide (DMSO), and dimethyl sulfone ($DMSO_2$).

Paper number 1999JD900083.
0148-0227/99/1999JD900083$09.00

Most anthropogenic sulfur is emitted into the atmosphere in the form of sulfur dioxide by activities such as fossil fuel combustion and biomass burning, although a small amount is emitted as sulfate as well. Volcanic activity is a small, but important, natural source of sulfur dioxide. The largest natural source of sulfur, however, is the flux of DMS from the oceans. The biosphere is also a source of a variety of reduced sulfur compounds. DMS is oxidized in the atmosphere by OH and NO_3 radicals to form sulfur dioxide as well as MSA and DMSO. Sulfur dioxide oxidation to form sulfate occurs either in the gas phase by the OH radical or in cloud droplets by hydrogen peroxide (H_2O_2) and, to a lesser extent, ozone. Predominant sinks of atmospheric sulfur include wet and dry deposition of sulfur dioxide and sulfate, leading to lifetimes of about a day, in the case of SO_2, and 4-6 days for sulfate. A significant amount of tropospheric sulfate occurs as part of the sea salt aerosol. These particles tend to be sufficiently large, however, that they have a much shorter lifetime. As a result, sea salt sulfate is typically excluded from consideration as a part of the tropospheric sulfur cycle.

Sulfate aerosols typically contain substantial amounts of condensable gases such as ammonia and nitric acid that exist in particle form as the ammonium, NH_4^+, and nitrate, NO_3^-, ions, respectively. Besides contributing to the total aerosol mass, the quantities of ammonium and nitrate in the sulfate aerosol affect the amount of water uptake at a given relative humidity, and also influence the optical properties of the aerosol via the

refractive index. The composition of the aerosol therefore plays an important role in both the direct and indirect effects on climate.

At thermodynamic equilibrium, the amount of water contained in an aerosol particle depends on temperature, relative humidity, and composition [*Seinfeld and Pandis,* 1998]. For example, at 298 K and 80% relative humidity the volume of an aqueous solution of sulfuric acid is about 5.5 times greater than its volume at 0% relative humidity, whereas the volume of an ammonium bisulfate particle is only 3.5 times greater. If metastable equilibria are considered, water uptake also depends on the history of the particle. The reason the particle's history plays a role in water uptake is because of the hysteresis effect in which the relative humidity required for a single-component dry solid particle to deliquesce is higher than the relative humidity at which an aqueous droplet crystallizes. The deliquescence and crystallization relative humidities depend, in turn, on particle composition. An ammonium sulfate particle crystallizes at 40% relative humidity, while ammonium bisulfate retains water to much lower relative humidities. For multicomponent mixtures the deliquescence and crystallization behavior is even more complex. Whereas the size a particle attains via uptake of water is influenced, as described above, by its composition, its refractive index is also determined by composition. Sulfuric acid is more hygroscopic than ammonium bisulfate or ammonium sulfate, but ammonium sulfate has the highest refractive index of the three. The overall climate forcing efficiency of sulfate aerosol increases with both water uptake and refractive index, so that the higher hygroscopicity of sulfuric acid is partly compensated by its lower refractive index and vice versa. For example, *Boucher and Anderson* [1995] found that at 80% relative humidity, the climate forcing efficiency of the sulfate ion is -132 W g^{-1} SO_4^{2-} for sulfuric acid, -104 W g^{-1} SO_4^{2-} for ammonium bisulfate, and -125 W g^{-1} SO_4^{2-} for ammonium sulfate. The degree to which sulfate is neutralized by ammonium therefore can influence its climate forcing efficiency by more than 25%.

Beyond modifying the hygroscopic and radiative properties of sulfate aerosol, ammonia and nitrate merit study for their own reasons. Ammonia is the only base present in sufficient quantities to neutralize a significant fraction of the sulfuric and nitric acids found in the troposphere. As such, it plays a key role in determining the pH of cloud condensation nuclei and precipitation. The pH of the atmospheric aqueous phase affects, in turn, the rates of several important chemical reactions. Since it has been estimated that the anthropogenic contribution to the ammonia budget is nearly 4 times the natural contribution [*Bouwman et al.,* 1997], this has created interest in two effects of ammonia and ammonium deposition on the biosphere. Such deposition increases the supply of fixed nitrogen available for plant growth and also, somewhat paradoxically, has been implicated in soil acidification [*Galloway,* 1995]. Finally, since the rate of nucleation of the ternary H_2SO_4-NH_3-H_2O system is estimated to be several orders of magnitude higher than that of the binary H_2SO_4-H_2O system [*Coffman and Hegg,* 1995], the rate of new particle formation in the presence of ammonia might be influential in the marine boundary layer.

Important anthropogenic sources of ammonia include emissions from domestic animals, fertilizer application, crops, and biomass burning [*Bouwman et al.,* 1997]. Emissions from the oceans, undisturbed soils, and natural vegetation are the primary natural emissions of ammonia. Once in the atmosphere, gaseous ammonia may absorb into the aerosol phase, especially in the presence of sulfate, to form the ammonium (NH_4^+) ion. Both ammonia and ammonium are removed from the atmosphere via wet and dry deposition. Like sulfur dioxide and sulfate, they have short lifetimes of about a day and between 4 and 6 days, respectively.

Aerosol nitrate is formed from nitric acid, which can dissolve directly in an aqueous aerosol solution or react with ammonia to form ammonium nitrate aerosol. Atmospheric nitric acid is the oxidation product of NO_x and is therefore found in areas with high emissions of NO_x. Fossil fuel combustion, release from soils, biomass burning, and lightning are the primary producers of NO_x. By serving as a reactive odd nitrogen (NO_y) reservoir, nitric acid couples aerosol dynamics to gas phase photochemistry. Modeling nitrate aerosol will allow this coupling to be examined in the future. Moreover, nitrate aerosol contributes to total aerosol radiative forcing on a regional basis. For example, radiative forcing attributable to nitrate alone has been estimated to be as large as -0.8 W m^{-2} in western Europe [*van Dorland et al.,* 1997].

The tropospheric sulfur cycle has been modeled extensively in global chemical transport models (CTMs) [*Erickson et al.,* 1991; *Langner and Rodhe,* 1991; *Pham et al.,* 1995; *Chin et al.,* 1996; *Kasibhatla et al.,* 1997], and also in general circulation models (GCMs) [*Penner et al.,* 1994; *Feichter et al.,* 1996; *Lelieveld et al.,* 1997; *Kjellstrom,* 1998; *Roelofs et al.,* 1998; Koch et al., Tropospheric sulfur simulation and sulfate direct radiative forcing in the GISS GCM, submitted to *Journal of Geophysical Research,* 1998, hereinafter referred to as Koch et al., submitted manuscript, 1998]. All of these studies focus on total mass concentration of sulfate particles, ignoring the ammonium, nitrate, and water that also comprise the aerosol.

Several studies have been made of both the direct and indirect radiative effects of sulfate aerosols. Studies of the direct effect may be roughly divided into two categories. In the first category [*Charlson et al.,* 1991; *Mitchell et al.,* 1995a, b; *Mitchell and Johns,* 1997] the direct effect of sulfate aerosol on the atmospheric radiation budget is parameterized as a change in the planetary reflectivity proportional to the sulfate burden [*Charlson et al.,* 1991]. In this category of studies, a uniform empirical value of the sulfate mass scattering coefficient is used. Assumptions about the size, composition, and water content of the sulfate aerosol are implicit in the choice of the value for the mass scattering coefficient, and therefore, using a uniform value ignores variation in these properties. In a second category of studies of the direct effect [*Kiehl and Briegleb,* 1993; *Haywood and Shine,* 1995; *Chuang et al.,* 1997; *Feichter et al.,* 1997; *Haywood et al.,* 1997; *van Dorland et al.,* 1997; *Haywood and Ramaswamy,* 1998], Mie theory is used to calculate the optical properties of the aerosol, which may then be used in a simple radiation scheme such as that of *Charlson et al.* [1991] or, more often, serve as input to a GCM radiation calculation. Aerosol optical properties depend on aerosol composition, size distribution, and water uptake. Table 1 summarizes various assumptions made in Mie theory calculations with regards to these aerosol properties. Typically, the aerosol has been assumed to follow a log normal size distribution. The degree to which sulfate is neutralized by ammonium has been assumed to be uniform throughout the troposphere, usually in the form of ammonium sulfate. Except for *van Dorland et al.* [1997], who assumed that 50% of boundary layer HNO_3 and 25% of free

Table 1. Summary of Assumptions Made About Aerosol Composition, Water Uptake, and Size Distribution in Calculations of Direct Radiative Forcing

Reference	Composition	RH	Hysteresis	Size Distribution
Chuang et al. [1997]	assumed $(NH_4)_2SO_4$	water uptake based on Kohler theory	optical properties averaged rising and falling RH cases	assumed lognormal r_m(dry)=0.05 μm σ=2.0
Feichter et al. [1997]	multiplied $[SO_4]$ by 1.46 to account for bound NH_4	assumed 80% constant		assumed lognormal r_m(dry)=0.07 μm σ=2.03
Haywood and Shine [1995]	assumed $(NH_4)_2SO_4$	uniform growth factor of 1.32		assumed lognormal r_m(dry)=0.05 μm σ=2.0
Haywood et al. [1997]	assumed $(NH_4)_2SO_4$	growth factor based on GCM RH	Three cases: ascending RH, descending RH, linear interpolation	assumed lognormal r_m(dry)=0.05 μm σ=2.0
Haywood and Ramaswamy [1998]	assumed $(NH_4)_2SO_4$	growth factor based on GCM RH	linear interpolation	assumed lognormal r_m(dry)=0.05 μm σ=2.0
Kiehl and Briegleb [1993]	assumed 75% H_2SO_4, 25% H_2O	*f*(RH) from observations, monthly mean RH from ECMWF		assumed lognormal r_m(dry)=0.05 μm σ=2.0
van Dorland et al. [1997]	assumed $(NH_4)_2SO_4$	Two cases: 80% constant; prescribed Oort [1983] in lower troposphere, fixed at 50% in upper troposphere		assumed lognormal r_m(dry)=0.021 μm σ=2.239

ECMWF, European Centre for Medium-Range Weather Forecasts; GCM, general circulation model; RH, relative humidity.

tropospheric HNO_3 occurs as nitrate aerosol with the same optical properties as sulfate, nitrate has been ignored in calculations of the global radiative effect of sulfate aerosols. Many of the studies treat water uptake by the aerosol as unvarying throughout the atmosphere, either by assuming a fixed relative humidity or by applying a uniform relative humidity growth factor. Therefore Mie theory calculations have also made assumptions about the composition and water content of the sulfate aerosol, and ignore spatial variations in these properties.

Previous work indicates that an online GCM model of sulfate composition, including explicit treatment of ammonium, nitrate, and water, will lead to more realistic estimates of the magnitude and distribution of direct radiative forcing than those that result from imposing assumptions of uniform composition and water uptake on sulfur-only concentration fields. For example, *van Dorland et al.* [1997] estimated that the global and annual average direct radiative forcing from sulfate aerosols is –0.36 W m^{-2} assuming a uniform relative humidity of 80%, but only –0.32 W m^{-2} taking into account local variations in relative humidity. Although this is a small effect when globally averaged, locally the effect of relative humidity was larger. Whereas the effect of relative humidity variations may be small when globally averaged, this averaging disguises large differences in the spatial distribution of forcing that cannot be determined by radiative calculations that assume a fixed relative humidity. As mentioned above, sensitivity tests on the ammonium content have shown that it has more than a 25% effect on sulfate forcing efficiency. Given the local variations in global ammonia emissions, this too could alter the spatial distribution of the forcing. Simulating aerosol composition and water uptake online in a GCM therefore can reduce uncertainties in calculating direct radiative forcing and generate a spatial distribution of forcing that realistically accounts for variations in aerosol properties.

Aerosol composition also plays a role in determining the magnitude of the indirect effect, although there are still too many unanswered questions for GCM estimates of the indirect effect to take account of this in a detailed way. One GCM study of climate response to indirect sulfate forcing arbitrarily chose a climate forcing of -4 W m^{-2} with a spatial distribution in proportion to local sulfate concentrations [*Erickson et al.*, 1995], while another study used satellite measurements of cloud droplet effective radii as input to a GCM [*Boucher*, 1995]. Most commonly, observational data are used to derive empirical relationships between cloud droplet number concentration and sulfate mass [*Jones et al.*, 1994; *Boucher and Lohmann*, 1995; *Feichter et al.*, 1997; *Lohmann and Feichter*, 1997]. Another method, in which the aerosol size distribution is determined by the fraction of anthropogenic sulfate formed via aqueous oxidation with the number of CCN depending on this size distribution, total number of aerosol particles, and the mean vertical velocity of the GCM, is described by *Chuang et al.* [1997]. No GCM study of the indirect effect therefore has considered aerosol composition as a variable, although water uptake by aerosol particles, and hence cloud droplet activation, depends on aerosol composition. Recent work [*Kulmala et al.*, 1993] also suggests that the presence of nitric acid can enhance cloud

droplet activation by contributing soluble material to aerosol particles. A GCM simulation of aerosol composition therefore lays the groundwork for a more thorough parameterization of the indirect effect in GCMs, although substantial work must still be done before this is feasible.

While several models of atmospheric ammonia on the regional scale exist [*Iversen et al.*, 1991; *Asman and van Jaarsveld*, 1992; *Fekete and Gyenes*, 1993; *Hov et al.*, 1994; *Galperin and Sofiev*, 1998; *Metcalfe et al.*, 1998; *Singles et al.*, 1998; *Syri et al.*, 1998], only one global modeling effort has been reported [*Dentener and Crutzen*, 1994] (hereinafter referred to as DC94). This study was the first to derive a 10° x 10° emissions inventory for ammonia and calculate global distributions of ammonia and ammonium using a three-dimensional model. It was limited, however, by coarse horizontal resolution and a thick boundary layer, as well as simple boundary layer and cloud parameterizations. It also treated condensation of ammonia on sulfate as a pseudo-first-order kinetic process and artificially imposed a maximum limit on neutralization of 1.5 mol of ammonium per mole of sulfate.

Radiative forcing attributable to nitrate aerosol was estimated by *van Dorland et al.* [1997], but they obtained their aerosol nitrate concentrations by assuming that 50% of all boundary layer and 25% of free tropospheric HNO_3 was present as accumulation mode nitrate aerosol. They found that the average radiative forcing in the Northern Hemisphere due to nitrate was about 10% of that due to sulfate, but more significant in localized regions such as western Europe. More recently, Metzger et al. (Aerosol multiphase equilibrium composition: A parameterization for global modeling, submitted to *Journal of Geophysical Research*, 1998, hereinafter referred to as Metzger et al., submitted manuscript, 1998) have used thermodynamic equilibrium to estimate the amount of particulate nitrate near the earth's surface in January and July based on average concentrations of sulfate, ammonia, and nitric acid taken from a CTM. To the best of our knowledge, however, no one has calculated the amount of particulate nitrate in a three-dimensional global model extending throughout the troposphere and covering the entire year.

In this study, we simultaneously model the transport of sulfur species, ammonium, and ammonia in a general circulation model and compute the ammonium, nitrate, and water content of sulfate aerosols according to thermodynamic equilibrium. Assuming thermodynamic equilibrium in each cell of the GCM allows us to understand how aerosol composition varies from region to region of the globe and also alleviates the necessity of arbitrarily specifying the ammonium to sulfate molar ratio.

The following section describes the GCM used in this study, the model of sulfur transport used as a starting point for this work, and the enhancements made to model aerosol composition. We then present and discuss simulated concentration fields of ammonia, ammonium, nitrate, and aerosol water content and compare them to available observations. Sensitivity studies are also analyzed to demonstrate how total aerosol mass is affected by the availability of various precursors. The final section summarizes important conclusions drawn from this work.

2. Model Description

2.1. GISS GCM II-Prime

Tracer transport is handled online in the Goddard Institute for Space Studies General Circulation Model II-prime (GISS GCM II-prime). A description of the older GISS GCM II is given by *Hansen et al.* [1983]; *Rind and Lerner* [1996] provide a discussion of recent improvements relevant to tracer studies. The resolution of the GISS GCM II-prime is 4° latitude by 5° longitude in the horizontal directions, with nine sigma layers in the vertical, from the surface to 10 mbar. The model surface layer is 50 mbar thick. The top one or two layers, centered around 27 and 103 mbar, are situated in the lower stratosphere. The model time step for tracer processes is 1 hour. The version of the GCM used in this study uses a quadratic upstream module for advection of heat and moisture, and a fourth-order scheme for tracer advection. The GCM carries liquid water as a prognostic variable in the large-scale cloud scheme [*Del Genio et al.*, 1996]. Moist convection is implemented by a variable mass flux scheme that includes two plumes, one entraining and one nonentraining, as well as a downdraft [*Del Genio and Yao*, 1993]. The boundary layer parameterization uses a new scheme that incorporates a finite modified Ekman layer [*Hartke and Rind*, 1997]. The improved parameterizations of these processes make this model especially suitable for studying aerosol sulfate, which resides mostly in the boundary layer and of which a substantial amount is formed via in-cloud oxidation.

2.2. Sulfur Cycle

An online sulfur model (Koch et al., submitted manuscript, 1998) that predicts the concentrations of SO_2, SO_4^{2-}, DMS, MSA, and H_2O_2 was used as the starting point for this work. Hydrogen peroxide is included as a prognostic species because it is depleted by reaction with SO_2 in heavily polluted areas during winter [*Chin et al.*, 1996]. This model includes Global Emissions Inventory Activity (GEIA) emissions of SO_2 and SO_4^{2-} from fossil fuel combustion and industrial activities, SO_2 emissions from biomass burning, aircraft, and noneruptive volcanoes, as well as an oceanic DMS source. SO_2 is oxidized in cloud by H_2O_2 and in the gas phase by the OH radical. Including H_2O_2 as a prognostic species has the effect of limiting the amount of SO_2 that oxidizes to SO_4^{2-} in polluted areas in the winter. As a result, less ammonia will condense into the aerosol phase so more gas phase ammonia will be available for the formation of ammonium nitrate. Both OH and NO_3 radicals oxidize DMS. Dry deposition of all species in the sulfur model, except DMS, uses a resistance-in-series parameterization [*Wesely and Hicks*, 1977] and is implemented as described by *Chin et al.* [1996], except that GCM surface momentum and heat fluxes are used to calculate the aerodynamic resistances. No subgrid deposition parameterization is used.

Wet deposition of dissolved tracers generally follows the GCM treatment of liquid water [*Del Genio and Yao*, 1993; *Del Genio et al.*, 1996]. The GCM distinguishes between large-scale and convective clouds. After reacting with each other, the remaining SO_2 and H_2O_2 dissolve into cloud water according to effective Henry's law coefficients assuming a pH of 4.5. Sulfate and MSA aerosols are assumed to be infinitely soluble. The GCM convective scheme considers both entraining and nonentraining plumes as well as compensating subsidence and downdrafts. All liquid water associated with convective clouds either precipitates, evaporates, or detrains into the large-scale cloud cover within the 1-hour time step of the model, and dissolved tracer species are either deposited or returned to the atmosphere in corresponding proportions. The large-scale cloud scheme of the GCM carries liquid cloud water content as a prognostic variable. Large-scale clouds

therefore may persist for several model time steps. Tracer budgets, on the other hand, do not distinguish between dissolved and undissolved tracer. Instead, tracers are scavenged in large-scale clouds according to a first-order rate loss parameterization that depends on the rate of conversion of cloud water into rainwater. Below both types of clouds, aerosols and soluble gases are scavenged according to a first-order parameterization that depends on the amount of precipitation. Dissolved tracer is also returned to the atmosphere if precipitation from either type of cloud evaporates.

The model year used for this study has an average sulfate burden of 0.73 Tg S. This value is intermediate in comparison with other sulfur models that exhibit burdens from 0.53 Tg S [*Chin et al.*, 1996] to 1.05 Tg S [*Lelieveld et al.*, 1997].

The model of sulfate composition has been developed by adding species to the sulfur model described above. Sulfur, ammonia, ammonium, and nitrate are all considered in the standard model run, while nitrate is omitted in a subsequent sensitivity run.

2.3. Ammonia Cycle

The ammonia cycle was simulated by adding two tracers: gas phase ammonia (NH_3) and aerosol ammonium (NH_4^+). Ammonia emissions were specified according to a recent GEIA inventory [*Bouwman et al.*, 1997]. The total ammonia source in this inventory was estimated to be 53.6 Tg N yr^{-1}, and Table 2 shows this total according to source type. Domestic animals contribute most to total emissions, followed by fertilizers, oceans, soils under natural vegetation, crops, and others. The fact that agricultural activities contribute most to ammonia emissions implies that densely populated regions tend to have the highest ammonia emissions. The geographic distribution of NH_3 emissions is shown in Plate 1. The strongest source regions occur in eastern China, India, Europe, the American Midwest, and southern Brazil. The total emissions estimate of the GEIA inventory used here is higher than the 45 Tg N yr^{-1} used by DC94 in their model of the ammonia cycle, lower than the 75 Tg N yr^{-1} estimate of *Schlesinger and Hartley* [1992], and practically the same as the 54 Tg N yr^{-1} estimate of *Warneck* [1988]. The GEIA inventory specifies the seasonality of the oceanic source only, leaving all other emissions estimates as annual averages. It is obvious, however, that ammonia emissions from crops and fertilizer application will occur overwhelmingly during the growing season. Ammonia volatilization from animal excreta increases with temperature [*Bouwman et al.*, 1997] and seasonal differences in waste management, animal housing, and urease activity could also lead to seasonality in emissions from domestic animals. Therefore, following DC94, a seasonal cycle was imposed on the domestic animals, fertilizers, and crops sources by weighting emissions by the number of daylight hours. While the choice of this scheme is completely arbitrary, in the absence of any more detailed information, this is the simplest way to achieve a plausible temporal distribution of ammonia emissions. The GEIA inventory specifies the oceanic flux as a function of location and month. This flux has been calculated assuming an atmospheric ammonia concentration of zero such that the 8.2 Tg N yr^{-1} represents the potential, rather than the net, oceanic emission of ammonia to the atmosphere. This is appropriate since the GCM calculates dry deposition of gas phase ammonia to the ocean surface. The uncertainty in the global annual emission of ammonia was estimated to be ± 25% [*Bouwman et al.*, 1997], and uncertainties on shorter spatial and temporal scales are expected to be larger. This should be kept in mind when evaluating model results.

Table 2. Global Ammonia Emissions by Source [*Bouwman et al.*, 1997]

Source	Emission, Tg N yr^{-1}
Domesticated animals	21.6
Fertilizers	9.0
Oceans	8.2
Biomass burning	5.9
Crops	3.6
Humans	2.6
Soils under natural vegetation	2.4
Other	0.4
Total	53.6

Atmospheric ammonia undergoes reaction with the OH radical according to [*DeMore et al.*, 1997]

$$NH_3 + OH \rightarrow NH_2 + H_2O$$

At 298 K, at an OH concentration of 5 x 10^5 molecules cm^{-3}, the lifetime of ammonia with respect to this reaction is about 150 days. As this lifetime is much longer than the actual lifetime of ammonia, this reaction plays only a very small role in the global ammonia budget. Nevertheless, this reaction is accounted for in the GCM using three-dimensional fields of 5-day average OH radical concentrations (C. Spivakovsky, personal communication, 1998). To account for the diel variation in OH radical concentrations, an instantaneous value is obtained by scaling the 5-day average value to the cosine of the solar zenith angle.

Both wet and dry deposition of ammonia and ammonium follow the sulfur model. For purposes of wet deposition, the effective Henry's law coefficient for ammonia in precipitation at an assumed pH of 4.5 is 3.3 x 10^6 M atm^{-1}. The necessary data to estimate the surface resistance for dry deposition of ammonia are given by *Wesely* [1989]. The deposition velocity of ammonium is assumed to be the same as that of sulfate. Ammonium, like sulfate, is assumed to be infinitely soluble in rainwater.

2.4. Timescales for Gas-Aerosol Equilibration

We assume that the volatile species ammonia and nitric acid achieve an equilibrium partitioning between gas and aerosol phases during the 1-hour model time step. Therefore mass transport between gas and aerosol phases is not considered in the simulations presented here. Detailed box model calculations [*Meng and Seinfeld*, 1996] have shown that the time required for a particle to achieve equilibrium with the gas phase depends primarily on its size. In general, ammonia reached gas-aerosol equilibrium with the accumulation mode sulfate particles that are the focus of this study in less than an hour. The time to reach equilibrium was somewhat longer than an hour for the lower aerosol concentrations encountered in remote marine regions. The same was true for nitric acid except at lower relative humidities, where the time to reach equilibrium was 1.59 and 1.24 hours for 60% and 50% relative humidity, respectively. This is only slightly longer than the model time step, so the assumption that gas-aerosol equilibrium is attained should not significantly compromise our results. Moreover, we can expect that the characteristic time for significant changes in GCM temperature, relative humidity, sulfate, or ammonia concentrations that perturb

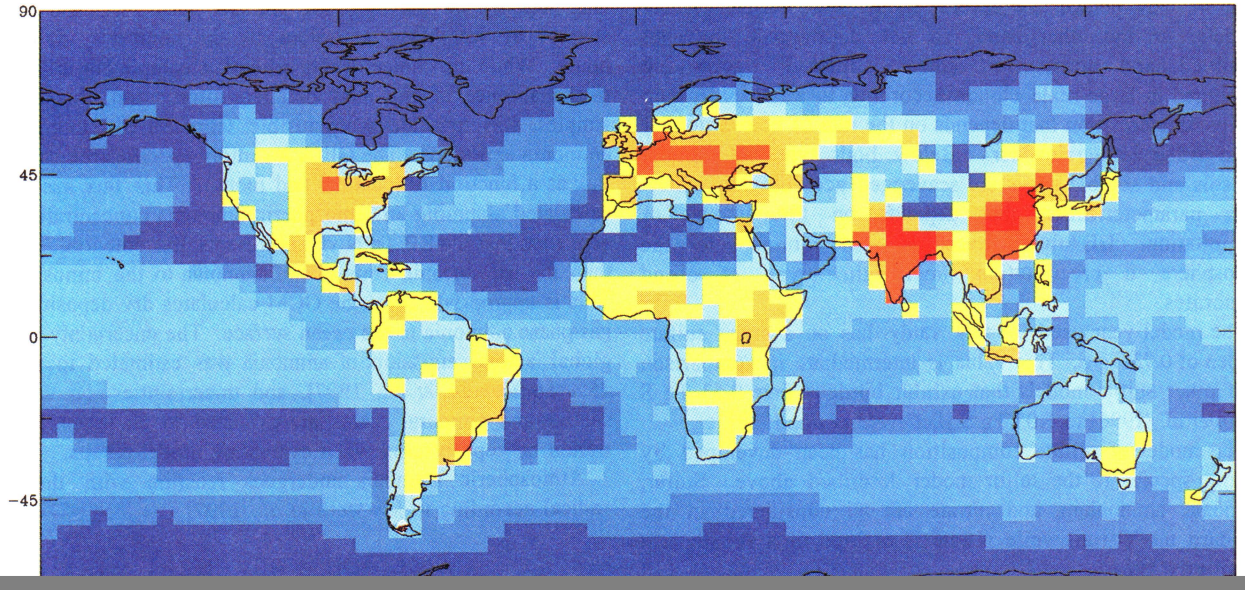
90
45
0
−45

therefore lie thermodynamically on the metastable branch of the aerosol activation hysteresis loop. As a result of this assumption, solid phases are not considered to be present during the equilibrium calculation. Even though this assumption has the side effect of forcing the aerosol phase to contain water even below the crystallization relative humidity, this situation occurs rarely because most sulfate mass resides in the humid midlatitudes, and the aerosol in the dry upper troposphere tends to contain ammonium bisulfate and unneutralized sulfuric acid, which remain in aqueous solution at very low relative humidities. Moreover, the mass of water forced into the aerosol phase below the crystallization relative humidity is small compared with the aerosol mass itself (about 7% of total aerosol mass for ammonium sulfate). With any solid phase species eliminated from consideration, as well as species containing sodium or chloride, the species considered in the equilibrium calculation are

Gas phase

NH_3, HNO_3, H_2O

Liquid phase

NH_4^+, H^+, NO_3^-, SO_4^{2-}, HSO_4^-, OH^-,H_2O

The equilibrium relations involving these species, applicable equilibrium constants at 298 K, and other relevant thermodynamic quantities are given in Table 3.

Tropospheric temperatures can range from 210 K to 320 K, and the temperature dependence of gas-aerosol equilibrium is important. ISORROPIA calculates the temperature dependence of equilibrium constants with the Van't Hoff equation,

$$\frac{d\ln K(T)}{dT} = \frac{\Delta H^0(T)}{RT^2} \tag{1}$$

where K is the equilibrium constant, T is the temperature (in Kelvins), R is the gas constant, and ΔH^0 is the standard enthalpy change of the reaction. The enthalpies of all species are assumed to vary linearly with temperature, on the basis of constant heat capacities. With this assumption the equilibrium constant is

$$K(T) = K_0 \exp\left[-\frac{\Delta H^0(T_0)}{RT}\left(\frac{T_0}{T}-1\right) - \frac{\Delta c_p^0}{R}\left(1+\ln\left(\frac{T_0}{T}\right)-\frac{T_0}{T}\right)\right] \tag{2}$$

where K_0 is the equilibrium constant at the reference temperature, T_0, and Δc_p^0 is the difference in heat capacities between products and reactants at the reference temperature. The equilibrium constant at the reference temperature is

Table 3. Equilibrium Relations and Constants Used in the Aerosol Thermodynamic Equilibrium Module ISORROPIA [*Nenes et al.*, 1998]

Reaction	Equilibrium Constant Expression	K_o (298.15K)	$\frac{\Delta H^0(T_0)}{RT_0}$	$\frac{\Delta c_p^0}{R}$	Units
$HSO_{4(aq)}^- \overset{K_1}{\longleftrightarrow} H_{(aq)}^+ + SO_{4(aq)}^{2-}$	$\frac{[H^+][SO_4^{2-}]}{[HSO_4^-]}\frac{\gamma_{H^+}\gamma_{SO_4^{2-}}}{\gamma_{HSO_4^-}}$	1.015×10^{-2}	8.85	25.14	mol kg^{-1}
$NH_{3(g)} \overset{K_{21}}{\longleftrightarrow} NH_{3(aq)}$	$\frac{[NH_{3(aq)}]}{P_{NH_3}}\gamma_{NH_3}$	5.764×10^{1}	13.79	-5.39	mol kg^{-1} atm^{-1}
$NH_{3(aq)} + H_2O_{(aq)} \overset{K_{22}}{\longleftrightarrow} NH_{4(aq)}^+ + OH_{(aq)}^-$	$\frac{[NH_4^+][OH^-]}{[NH_{3(aq)}]a_w}\frac{\gamma_{NH_4^+}\gamma_{OH^-}}{\gamma_{NH_3}}$	1.805×10^{-5}	-1.50	26.92	mol kg^{-1}
$HNO_{3(g)} \overset{K_4}{\longleftrightarrow} H_{(aq)}^+ + NO_{3(aq)}$	$\frac{[H^+][NO_3^-]}{P_{HNO_3}}\gamma_{H^+}\gamma_{NO_3^-}$	2.511×10^{6}	29.17	16.83	mol^2 kg^{-2} atm^{-1}
$H_2O_{(aq)} \overset{K_w}{\longleftrightarrow} H_{(aq)}^+ + OH_{(aq)}^-$	$\frac{[H^+][OH^-]}{a_w}\gamma_{H^+}\gamma_{OH^-}$	1.010×10^{-14}	-22.52	26.92	mol^2 kg^{-2}
$(NH_4)_2SO_{4(s)} \overset{K_7}{\longleftrightarrow} 2NH_{4(aq)}^+ + SO_{4(aq)}^{2-}$	$[NH_4^+]^2[SO_4^{2-}]\gamma_{NH_4^+}^2\gamma_{SO_4^{2-}}$	1.817×10^{0}	-2.65	38.57	mol^3 kg^{-3}
$NH_4NO_{3(s)} \overset{K_{10}}{\longleftrightarrow} NH_{3(g)} + HNO_{3(g)}$	$P_{NH_3}P_{HNO_3}$	5.746×10^{-17}	-74.38	6.12	atm^2
$NH_4HSO_{4(s)} \overset{K_{12}}{\longleftrightarrow} NH_{4(aq)}^+ + HSO_{4(aq)}^-$	$[NH_4^+][HSO_4^-]\gamma_{NH_4^+}\gamma_{HSO_4^-}$	1.383×10^{0}	-2.87	15.83	mol^2 kg^{-2}
$(NH_4)_3H(SO_4)_{2(s)} \overset{K_{13}}{\longleftrightarrow}$	$[NH_4^+]^3[SO_4^{2-}][HSO_4^-]x$	2.972×10^{1}	-5.19	54.40	mol^5 kg^{-5}
$3NH_{4(aq)}^+ + HSO_{4(aq)}^- + SO_{4(aq)}^{2-}$	$\gamma_{NH_4^+}^3\gamma_{SO_4^{2-}}\gamma_{HSO_4^-}$				

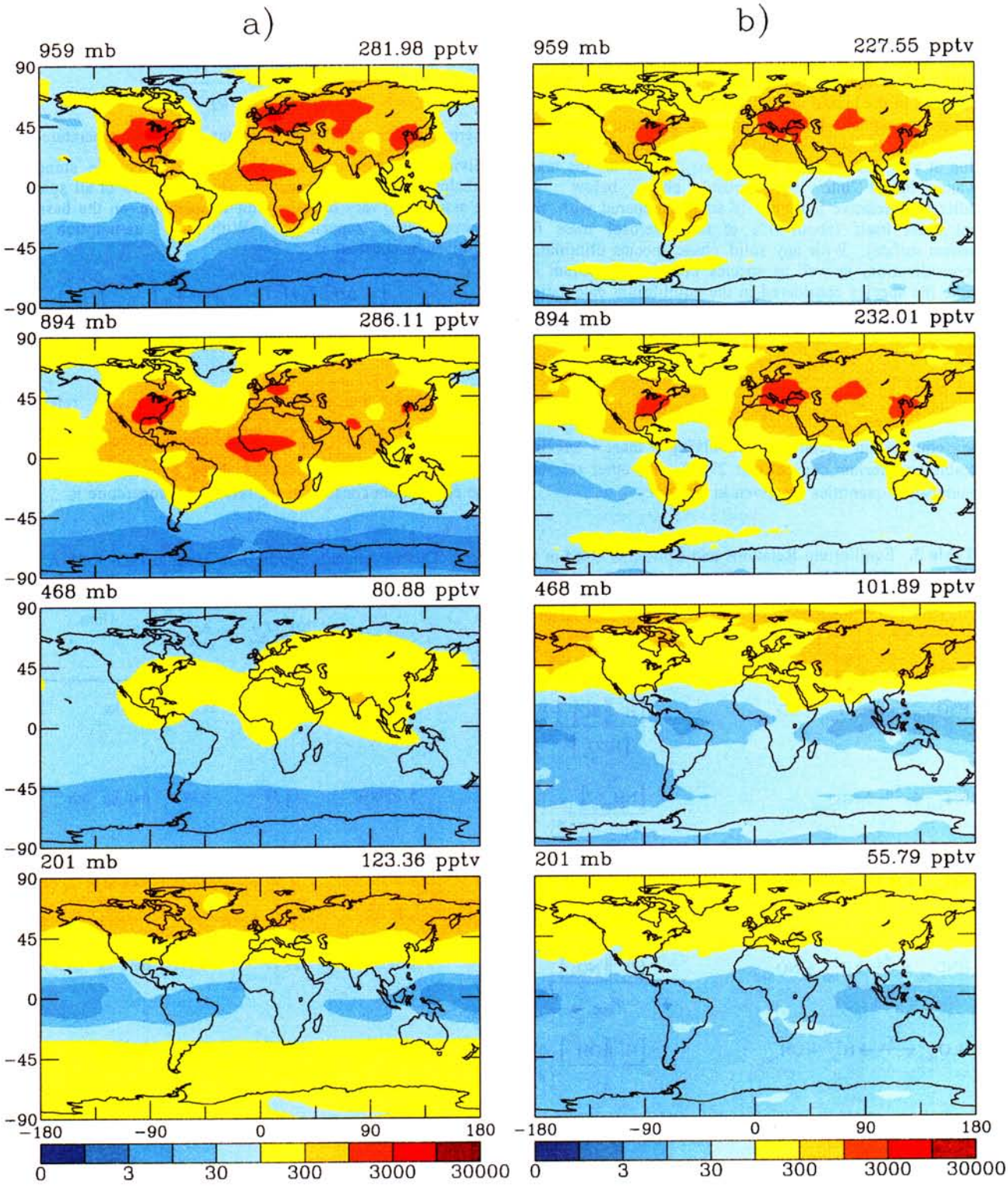

Plate 2. (a) Annual average of monthly nitric acid mixing ratio fields used as input by the GCM. (b) Annual average sulfate mixing ratios. Note that 1 μg m^{-3} SO_4^{2-} = 258 pptv SO_4^{2-} at 298 K and 1 bar. Above each plot, the pressure level of the corresponding model layer is indicated, as is the average mixing ratio in that layer. Contour lines are 1, 3, 10, 30, 100, 300, 1000, 3000, 10,000, and 30,000 pptv.

Table 4. Thermodynamic Properties in the Aerosol Thermodynamic Equilibrium Module, ISORROPIA [*Nenes et al.*, 1998]

Species	ΔG_f^0, kJ mol^{-1}	ΔH_f^0, kJ mol^{-1}	c_p^0, J mol^{-1} K^{-1}
$HNO_{3\,(g)}$	-74.720	-135.060	53.350
$NH_{3\,(g)}$	-16.450	-46.110	35.060
$H^+_{(aq)}$	0.000	0.000	0.000
$NH_4^+{}_{(aq)}$	-79.310	-132.510	79.900
$HSO_4^-{}_{aq)}$	-755.910	-887.340	-84.000
$SO_4^{2-}{}_{(aq)}$	-744.530	-909.270	-293.000
$NO_3^-{}_{(aq)}$	-111.250	-207.360	-86.600
$OH^-_{(aq)}$	-157.244	-229.994	-148.500

$$K_0 = \exp\left[-\frac{\sum_i \nu_i \mu_i^0(T_0)}{RT_0}\right] \quad (3)$$

In this expression, ν_i is the stoichiometric coefficient of the ith species in the equilibrium relation, and μ_i^0 is its chemical potential at the reference temperature. The Gibbs free energy of formation, enthalpy of formation, and heat capacity of each species are given in Table 4.

An example of characteristic behavior of the sulfate-nitrate-ammonium aerosol system is shown in Figure 1. The predictions show how equilibrium aerosol composition varies as a function of total sulfate mass at 285 K and 80% relative humidity. The calculation was carried out assuming a fixed total mass of 4.5 μg m^{-3} of ammonia and 6.0 μg m^{-3} of nitric acid. Sulfate has a sufficiently low vapor pressure that it can be assumed to reside completely in the aerosol phase. Ammonia and nitric acid, on the other hand, partition themselves between both gas and aerosol phases. At these conditions, nitric acid can exist in the aerosol phase in the form of the nitrate ion, but only when neutralized by ammonium. At low sulfate concentrations the ammonium nitrate aerosol represents about a third of the total ammonia in the system and nearly all of the nitric acid. Ammonium concentrations increase with increasing sulfate concentrations until essentially all the ammonia is drawn into the aerosol phase. At this point, because of the lack of free ammonia, additional sulfate tends to force nitrate out of the aerosol phase. As a result of the thermodynamic competition between sulfate and nitrate, the total aerosol mass, dry or wet, is a nonlinear function of the amount of sulfate in the system.

2.6. Aerosol Nitrate

Aerosol nitrate was generated by providing the thermodynamic equilibrium module with total (gas plus aerosol) concentrations of nitric acid. The resulting concentrations of aerosol nitrate were stored as model output but were not allowed to undergo advection or deposition. In a sensitivity run, nitric acid concentrations were taken to be zero. A limitation of the nitrate simulation presented here is that neither sea salt nor mineral dust is included. Since both these types of aerosols are known to take up nitrate from the gas phase [*Tabazadeh et al.*, 1998], we expect to underestimate particulate nitrate concentrations wherever these processes are important. The aerosol nitrate concentrations calculated here represent therefore the sum of ammonium nitrate and dissolved nitric acid and neglect species such as $NaNO_3$ and $Ca(NO_3)_2$.

We use three-dimensional monthly average nitric acid concentration fields taken from the Harvard CTM photochemical model, which uses an archived meteorology based on the GISS GCM II [*Horowitz et al.*, 1998; Horowitz and Jacob, Global impact of fossil fuel combustion on atmospheric NO_x, submitted to *Journal of Geophysical Research*, 1999]. Plate 2a shows the annual average of these monthly fields for selected model layers. Although the Harvard CTM accounts for both heterogeneous and gas phase production of nitric acid, all nitric acid is assumed to reside in the gas phase for purposes of deposition. Since gas phase nitric acid tends to undergo dry deposition more rapidly than particulate nitrate, the CTM may overestimate somewhat the dry deposition of total nitric acid.

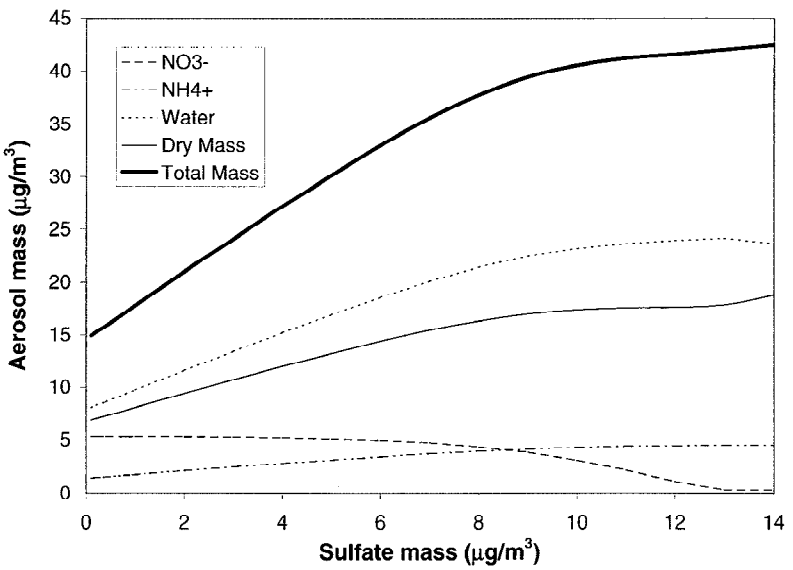

Figure 1. Mass concentration of various aerosol components as a function of sulfate mass. These results were calculated by the aerosol thermodynamic equilibrium module, ISORROPIA, for 285 K, 80% relative humidity, 4.5 μg m^{-3} total NH_3, and 6.0 μg m^{-3} total HNO_3.

Horowitz et al. [1998] reported that simulated HNO_3 concentrations were about 25% larger than observed concentrations at the three North American sites that were used for comparison. Two reasons for this discrepancy were suggested. First, HNO_3 undergoes rapid dry deposition, resulting in a strong vertical gradient near the surface. One therefore expects that model predictions, which reflect conditions throughout the lowest 500 m of the atmosphere, should exceed observed concentrations at the surface. Second, CTM HNO_3 is the sum of gas phase nitric acid and aerosol nitrate, whereas the observations are of gas phase nitric acid only. This suggests that the Harvard CTM nitric acid fields used in this study are within 25% of actual values for North America, although this conclusion is based on observations at only three sites. Predictions in the remote troposphere are frequently several times larger than observations. Moreover, no comparison with European observations of HNO_3 has been made. In light of the above, it must be concluded that the HNO_3 concentration fields used as input, although the best currently available, represent a potentially considerable source of uncertainty. It is likely that HNO_3 predictions are too high, especially in remote areas, and could result in an overprediction of nitrate aerosol concentrations. Fortunately, this problem is mitigated by the fact that ammonium nitrate formation in remote areas is limited by the availability of ammonia.

The equilibrium water content of the aerosol was also tracked by the model. As with particulate nitrate, aerosol water was not allowed to undergo tracer transport.

All simulations were integrated over 13 months starting from zero concentrations. Data from the first month were ignored to allow the model to spin-up. Unless otherwise specified, all results shown here are annual averages over the remaining 12 months.

3. Global Aerosol Concentration Fields

This section presents predicted aerosol concentration fields, as well as several derived fields that highlight interactions among various species, such as the degree of aerosol neutralization. Aerosol concentrations and compositions have been compared with several observational databases. These databases will first be described.

3.1. Observational Data Sets

From June 1988 to May 1990, participants in the Eulerian Model Evaluation Field Study (EMEFS), took daily aerosol measurements at approximately 130 sites spread throughout eastern North America [*McNaughton and Vet,* 1996]. We have computed annual average sulfate, ammonium, and nitrate concentrations for 75 of these locations, and gas phase ammonia concentrations have been computed for 59 sites. Table 5 lists the EMEFS sites as well as observed and simulated annual mean mixing ratios. The long-term nature of the observations, inclusion of all the major aerosol ions and ammonia, and the large number of sampling locations (including several instances of more than one sampling location in a GCM grid cell) make this database an excellent test of model performance in eastern North America.

Aerosol composition data for Europe have been made available under the auspices of the Co-operative Programme for Monitoring and Evaluation of the Long-Range Transmission of Air Pollutants in Europe (European Monitoring and Evaluation Programme, EMEP) from 1986 to 1995 [*Hjellbrekke and Hanssen,* 1998]. Realizing that it is not feasible for our simulation, which is based on fixed emissions inventories, to accurately represent a 10-year period during which emissions changed, we compare our model predictions only with data taken during 1990. This year was chosen because it is the year in which simulated sulfate concentrations most closely match reported values. This facilitates comparison of other simulated aerosol components with observations, since errors in the sulfate simulation only compound errors and uncertainties in the treatment of other components. Fourteen EMEP sites reported annual average aerosol composition data for 1990, though not all sites reported data for all species. Table 6 shows these locations along with observed and simulated mixing ratios. Although the subset of the EMEP database used here is not as extensive as that of EMEFS, it still includes a reasonable number of long-term observations for sulfate and ammonium. The small number of ammonia and nitrate observations, however, makes assessment of model performance in Europe with respect to these species preliminary.

Since the sites that contributed to the two databases just described are all in or near industrialized regions, an effort was made to supplement these data with observations in other regions of the globe. DC94 compared their simulated sulfate and ammonium concentrations with a set of observed concentrations taken from the literature. We have extended this set to include a larger number of sites, as well as to include aerosol nitrate and gas phase ammonia. Many of these observations were taken in marine and remote continental areas, and the inclusion of aircraft observations helps to evaluate model behavior in the boundary layer and free troposphere. A major drawback of these data is that the vast majority of them were gathered over only relatively short time periods, usually a few days or weeks, and strongly reflect the prevailing meteorological conditions. One must bear this in mind when comparing these data with GCM-simulated concentrations, which are not based on the same meteorology. Because these observations were taken at a wide variety of sites, they have been divided into three categories: polluted continental, remote continental, and marine. The observations, with corresponding simulated values, are given in Table 7.

3.2. Sulfate

Results of the sulfur model used in this work have already been presented and compared with observations [Koch et al., submitted manuscript, 1998]. Therefore we will present here only the sulfate results that are necessary for understanding the behavior of the other aerosol components that are the focus of this study. Annual average sulfate mixing ratios for selected GCM layers are shown in Plate 2b. The highest sulfate mixing ratios occur in the industrialized areas of Europe, North America, and eastern Asia, where they exceed 1 ppbv (1 $\mu g\ m^{-3}$ SO_4^{2-} = 258 pptv SO_4^{2-} at 298 K and 1 bar). Sulfate mixing ratios also exceed 1 ppbv in central Asia as a result of transport of sulfur species from Europe as well as local anthropogenic sources. Sulfate mixing ratios in remote continental areas range from 30 pptv to 300 pptv. Marine mixing ratios generally exceed 100 pptv in the Northern Hemisphere and are lower in the Southern Hemisphere. The lowest sulfate mixing ratios, less than 30 pptv, occur in the remote Pacific and Indian Oceans, mostly in the southern tropics. Sulfate mixing ratios are fairly uniform with altitude

Table 5. Comparison of Simulated and Observed Mixing Ratios From the EMEFS Database

Location	Latitude, °N	Longitude, °W	SO_4^{2-}		NO_3^-		NH_4^+		NH_3	
			Obs	Sim	Obs	Sim	Obs	Sim	Obs	Sim
Algoma, Ontario	47	84	664	1058	167	494	999	1656		334
Archbold, Florida	27	81	762	568	444	6	1107	664	1369	169
Arendtsville, Pennsylvania	40	77	1750	1739	848	614	3543	2514	581	426
Balsam Lake, Ontario	45	79	959	933	419	628	1594	1733		464
Bells, Tennessee	36	89	1337	1851	422	393	2250	2415	771	577
Benton, Kentucky	37	88	1753	2094	447	957	2787	3509	422	854
Big Moose, New York	44	75	969	1169	121	850	1463	2395	84	656
Brackney, Pennsylvania	42	76	1376	1613	316	1145	2230	3169	122	613
Brokensword, Ohio	41	83	1535	1892	1100	1219	3584	3568	823	730
Brookings, South Dakota	44	97	566	550	639	1086	1459	2016	3332	2048
Cadiz, Kentucky	37	88	1635	2094	445	957	3005	3509	1044	854
Caryville, Florida	31	86	1091	1153	228	72	1670	1285	371	228
Cedar Creek SP, West Virginia	39	81	1681	2271	130	746	2126	3069	70	443
Chalk River, Ontario	46	77	852	933	97	628	1163	1733		464
Chapais, Quebec	50	75	456	431	25	232	461	656		213
Charleston Lake, Ontario	45	76	711	933	274	628	1361	1733		464
Coweeta Forest, North Carolina	35	83	1311	1696	77	247	1696	2000	73	373
Cree Lake, Saskatchewan	57	107	242	317	23	110	250	399		111
Decatur, Pennsylvania	41	77	1561	1613	716	1145	3451	3169	1782	613
Deer Cr. Park, Ohio	40	83	1847	2271	892	746	3779	3069	574	443
Dorset, Ontario	45	79	819	933	197	628	1263	1733		464
Due West, South Carolina	34	82	1508	1696	229	247	2411	2000	355	373
E. Smithfield	42	77	1377	1613	553	1145	2829	3169	1142	613
E.L.A., Ontario	50	94	380	438	130	462	579	1038		551
Eddyville, Kentucky	37	88	1707	2094	452	957	2782	3509	242	854
Egbert, Ontario	44	80	1098	933	921	628	2472	1733	1010	464
Emporium, Pennsylvania	42	78	1421	1613	220	1145	1893	3169	57	613
Fernberg, Minnesota	48	91	358	639	184	1158	640	2167		1732
Ford City, Pennsylvania	41	80	1745	1613	405	1145	2909	3169	292	613
Fort Wayne, Indiana	41	85	1627	1449	1303	1548	3793	3524	1157	1149
Gaylord, Michigan	45	85	923	1058	298	494	1571	1656	250	334
Gowganda, Ontario	48	81	563	1058	89	494	808	1656		334
Hawthorne, Pennsylvania	41	79	1688	1613	328	1145	2622	3169	101	613
High Falls, Ontario	46	82	682	1058	148	494	1014	1656		334
Ithaca, New York	42	76	1290	1613	330	1145	2220	3169	133	613
Jerome, Missouri	38	92	1068	1546	326	1114	1873	3154	561	1532
Kane Forest, Pennsylvania	42	79	1481	1613	246	1145	2087	3169	47	613
Kejimkujik, Nova Scotia	44	65	734	608	90	262	680	965		297
Lancaster, Kansas	40	95	840	780	804	678	1686	2020	3080	2144
Leitchfield, Kentucky	37	86	1866	2094	479	957	3225	3509	399	854
LilleyCornett, Kentucky	37	83	1625	2271	177	746	2014	3069	263	443
Little Marsh, Pennsylvania	42	77	1390	1613	298	1145	2318	3169	165	613
Longwoods, Ontario	43	81	1266	1892	1056	1219	2769	3568		730
Marion, Alabama	33	87	1342	1851	235	393	2089	2415	510	577
Marshall, Texas	33	94	1320	1311	309	485	1884	2123	346	975
Montmorency, Quebec	47	71	630	760	54	696	833	1679		604
Moorhead, Kentucky	38	84	1929	2271	279	746	2689	3069	144	443
Morton, Mississippi	32	90	1210	1851	374	393	2364	2415	3143	577
Mountain Lake, Virginia	37	81	1733	2271	171	746	1892	3069	66	443
New Concord, Kentucky	37	88	1710	2094	271	957	2312	3509	164	854
North Orwell, Pennsylvania	42	76	1380	1613	430	1145	2490	3169	189	613
Parsons, West Virginia	39	80	1827	1739	245	614	2357	2514	165	426
Penn State, Pennsylvania	41	78	1626	1613	336	1145	2572	3169	125	613
Perryville, Kentucky	38	85	1936	2271	479	746	3222	3069	294	443
Piseco, New York	43	75	925	1169	118	850	1368	2395	52	656
Pittsboro, North Carolina	36	79	1561	1049	362	112	2825	1115	677	204
Renovo, Pennsylvania	41	78	1517	1613	238	1145	2075	3169	52	613
Roaring Creek, North Carolina	36	82	1439	2271	117	746	1613	3069	61	443
Round Lake, Wisconsin	46	92	571	639	361	1158	1230	2167	440	1732
Shawano, Wisconsin	45	89	880	874	1017	673	2524	1880	2715	701
Sutton, Quebec	45	73	984	760	228	696	1781	1679		604
Tunkhannock, Pennsylvania	42	76	1475	1613	349	1145	2514	3169	234	613
Underhill, Vermont	45	73	949	760	138	696	1454	1679	158	604
Uvalda, Georgia	32	82	1154	1696	263	247	1745	2000	357	373
Vincennes, Indiana	39	87	1731	2094	925	957	3371	3509	1038	854

Table 5. (Continued)

Location	Latitude °N	Longitude °W	SO_4^{2-} Obs	SO_4^{2-} Sim	NO_3^- Obs	NO_3^- Sim	NH_4^+ Obs	NH_4^+ Sim	NH_3 Obs	NH_3 Sim
Wartburg, Tennessee	36	85	1726	2271	238	746	2691	3069	196	443
Warwick, Massachusetts	43	72	1127	1169	159	850	1622	2395	127	656
Wayland, New York	43	78	1307	1613	433	1145	2479	3169	351	613
Wellesley, Ontario	43	81	1164	1892	1325	1219	3078	3568		730
Whiteface, New York	44	74	885	760	108	696	1201	1679	57	604
Williamsport, Pennsylvania	41	77	1599	1613	625	1145	3064	3169	338	613
Winterport, Maine	45	69	806	608	122	262	1146	965	118	297
Wirt, New York	42	78	1358	1613	249	1145	2016	3169	127	613
Yampa, Colorado	40	107	279	440	73	211	467	764	527	261
Zanesville, Ohio	40	82	1803	1892	644	1219	3130	3568	531	730

Mixing ratios are in parts per trillion by volume. EMEFS, Eulerian Model Evaluation Field Study.

throughout the boundary layer, but decrease in the free troposphere, with the average mixing ratio at the tropopause being about 25% of the surface layer value.

Figure 2 shows scatterplots of simulated sulfate mixing ratios versus observed values for each of the databases described above. In order to evaluate whether or not the model has a tendency to overpredict or underpredict aerosol concentrations, we took the geometric mean of the ratios of simulated values to observed values at each data point. The geometric mean ratio for each data set is shown in the corresponding scatter plot, and Table 8 shows the computed geometric mean for each data set and species. The model is able to predict annual average sulfate mixing ratios to within a factor of 2 at all the EMEFS and EMEP sites, although it tends to be about 15% high on average in North America. Comparison of simulated sulfate mixing ratios with the other data sets shows several locations where there is more than a factor of 2 discrepancy, but greater variation is expected from these observed concentrations, as they were collected over short time periods.

3.3. Ammonia

Annual average mixing ratios of gas phase ammonia at selected model layers are shown in Plate 3a. The highest surface mixing ratios, in excess of 3 ppbv (1 μg m^{-3} NH_3 = 1457 pptv NH_3 at 298 K and 1 bar), are found in India, China, eastern Europe, and Brazil. Continental mixing ratios exceed 100 pptv everywhere except the Arctic, western Sahara, and southwestern Australia. Marine concentrations are highest near the equator as a result of high ammonia emissions in that part of the ocean; otherwise, they are less than 100 pptv. Ammonia mixing ratios are negligibly small (less than 1 pptv) over most of Antarctica and only 3 to 10 pptv in the middle of the oceanic gyres. Emissions of ammonia and uptake by sulfate are the two factors that most strongly determine surface concentrations. Ammonia concentrations decline much more rapidly with altitude than do sulfate concentrations; the average mixing ratio at the tropopause is only 1% of the surface layer value, but concentrations are most persistent above India.

Annual average mixing ratios of particulate ammonium are shown in Plate 3b. Industrialized areas with high sulfate concentrations, such as the eastern United States, Europe, and China, tend to exhibit the largest ammonium mixing ratios, over 3 ppbv (1 μg m^{-3} NH_4^+ = 1377 pptv NH_4^+ at 298 K and 1 bar). Whereas mixing ratios in the Southern Oceans tend to fall in the 30-100 pptv range, they are 100-300 pptv in the northern oceans. Continental mixing ratios generally exceed 300 pptv. The lowest mixing ratios are found in Antarctica and the remote Pacific, where they range from 10 to 30 pptv. Ammonium mixing ratios at the tropopause are, on average, 16% of those at the surface. The decline in ammonium concentrations with altitude therefore is stronger than that of sulfate, but not as steep as that of ammonia.

The explanation for the stronger decline with altitude in ammonia and ammonium concentrations than for sulfate is that ammonia sources are located exclusively at the surface, while sulfate is produced chemically throughout the troposphere, although it has its own vertical gradient due to the distribution of its precursor, SO_2 [*Dentener and Crutzen,*

Table 6. Comparison of Simulated and Observed Mixing Ratios [pptv] from the EMEP Database

Location	Latitude	Longitude	SO_4^{2-} Obs	SO_4^{2-} Sim	NO_3^- Obs	NO_3^- Sim	NH_4^+ Obs	NH_4^+ Sim	NH_3 Obs	NH_3 Sim
Bilthoven, Netherlands	52° N	5° E	1138	984	1910	2008		3553		2214
Ispra, Italy	46° N	9° E	1447	1220	2440	1253	4687	2833		1057
Janiskoski, Russia	69° N	29° E	442	368	64	66	433	332		88
Jarczew, Poland	51° N	22° E	2360	1668		1727	3676	4354		2507
Kosetice, Czech Rep.	50° N	15° E	1798	2251	738	2029	2392	5601	10915	2197
K-puszta, Hungary	47° N	20° E	1489	2001	562	985	1910	4052	1541	1599
La Cartuja, Spain	37° N	4° W	1039	728		75	514	1224		915
Logrono, Spain	42° N	2° W	850	953		351	722	1715		800
Roquetas, Spain	41° N	1° W	969	953		351	867	1715		800
Suwalki, Poland	54° N	23° E	1608	1418		1722	1605	4014		2473
Svratouch, Czech Rep.	50° N	16° E	1475	2251	658	2029	4623	5601	12119	2197
Toledo, Spain	40° N	4° W	471	728		75	578	1224		915
Vysokoe, Belarus	52° N	23° E	1022	1418	742	1722	2263	4014		2473
Witteveen, Netherlands	53° N	7° E	976	984	1525	2008		3553		2214

Table 7. Comparison of Simulated and Observed Global Mixing Ratios

Location	Latitude	Longitude	Altitude	Time	SO_4^{2-} Obs	SO_4^{2-} Sim	NO_3^- Obs	NO_3^- Sim	NH_4^+ Obs	NH_4^+ Sim	NH_3 Obs	NH_3 Sim	Reference
Polluted Continental Sites													
Agra, India	27 N	78 E	surf	Dec-Mar	3526	278		31	8344	601		9914	*Kulshrestha et al.* [1998]
Allegheny Mountain, Pennsylvania	41.5 N	78.5 W	surf	Jun-Aug	4494	2298	202	537	3865	3181		615	*Pierson et al.* [1989]
Beijing	40 N	116 E	surf	Oct	2050	768		929	2800	2295		3308	*Huebert et al.* [1988]
Boulder, Colorado	40 N	105 W	surf	Jan-Dec	281	423		497	600	1209		1289	*Langford, et al.* [1992]
Boulder, Colorado	40 N	105 W	surf	Jun-Aug	382	540	517	326	989	1318	5169	1932	*Langford, et al.* [1992]
Boulder, Colorado	40 N	105 W	surf	Dec-Feb	180	213	315	724	652	1044	1348	558	*Langford, et al.* [1992]
Changsha	28 N	113 E	surf	Oct	2050	1872		804	3880	4433		7696	*Huebert et al.* [1988]
England	52 N	3 E	surf	Jan-Dec	1100	954		975	2500	2373		567	*Hansen, et al.* [1990]
Farkasfa, Hungary	47 N	16.5 E	surf	Jan-Dec	2161	2001	1459	985	4650	4052		1599	*Meszaros and Horvath,* [1984]
Germany	53 N	10 E	surf	Jan-Dec		1245		2072	3400	4106		2026	*Lenhard and Gravenhorst,* [1980]
Hungary	47 N	20 E	surf	Jan-Dec	2500	1561		1102	1600	3665		2740	*Hanssen et al.* [1990]
Kinterbish, Alabama	32.3 N	88.2 W	surf	Jun-Aug	1258	2767	202	13	1955	2339	629	438	*Langford, et al.* [1992]
K-puszta, Hungary	47 N	19.3 E	surf	Jan-Dec	2060	2001	1568	985	4730	4052	1561	1599	*Meszaros and Horvath,* [1984]
Lake Isabella, California	35.6 N	118.5 W	surf	Dec-Feb	90	326	202	339	180	796	427	365	*Jacob et al.* [1986]
Lake Ozette	47 N	125 W	surf	Mar-May	100	540		80	110	684		293	*Covert,* [1988]
Lancaster, England	54 N	3 W	surf	Jan-Dec	1978	800	2291	926	5571	2092		822	*Harrison and Pio,* [1983]
Los Angeles, California	34 N	118 W	surf	Nov-Dec	1676	332		231	18113	764		575	*John et al.* [1990]
Los Angeles, California	34 N	118 W	surf	Jun-Aug	2247	311		5	12125	570		765	*John et al.* [1990]
Newtown, Connecticut	41.5 N	73.5 W	surf	Jun-Aug	1461	1849	112	331	2517	2503	764	570	*Keeler et al.* [1991]
Northern Michigan	45 N	85 W	surf	Dec-Feb	629	619	427	1409	966	2291	45	417	*Cadle et al.* [1985]
Oak Ridge, Tennessee	36 N	84 W	surf	Jun-Aug	3978	3858	539	177	5393	3107	202	351	*Langford, et al.* [1992]
Oak Ridge, Tennessee	36.1 N	84.2	surf	Jun-Aug	2337	3858	67	177	2989	3107	337	351	*Lindberg et al.* [1990]
Poona, India	19 N	74 E	surf	Jan-Dec	440	408		14	980	800		3940	*Khemani et al.* [1982]
Sapporo, Japan	43 N	141 E	surf	Aug	895	1146	55	21	1268	1595		436	*Ohta and Okita,* [1990]
Sapporo, Japan	43 N	14 E	surf	Sep	701	676	172	18	823	977		176	*Ohta and Okita,* [1990]
Sapporo, Japan	43 N	141 E	surf	Apr	1277	1186	607	159	1376	1789		500	*Ohta and Okita,* [1990]
Sapporo, Japan	43 N	141 E	surf	Jul	1118	1000	43	48	1363	1565		552	*Ohta and Okita,* [1990]
Sapporo, Japan	43 N	141 E	surf	Jun	1032	735	204	68	1255	1146		454	*Ohta and Okita,* [1990]

Table 7. (Continued)

Location	Latitude	Longitude	Altitude	Time	SO_4^{2-} Obs	SO_4^{2-} Sim	NO_3^- Obs	NO_3^- Sim	NH_4^+ Obs	NH_4^+ Sim	NH_3 Obs	NH_3 Sim	Reference
Sapporo, Japan	43 N	141 E	surf	Oct	837	584	415	37	998	820		265	*Ohta and Okita,* [1990]
Sapporo, Japan	43 N	141 E	surf	Jan-Dec	1074	734	374	87	1546	1124		589	*Ohta and Okita,* [1990]
Sapporo, Japan	43 N	141 E	surf	Mar	1351	899	603	134	2320	1495		1031	*Ohta and Okita,* [1990]
Sapporo, Japan	43 N	141 E	surf	May	1166	742	466	89	1282	1138		417	*Ohta and Okita,* [1990]
Sapporo, Japan	43 N	141 E	surf	Nov	992	582	431	81	1538	815		456	*Ohta and Okita,* [1990]
Sapporo, Japan	43 N	141 E	surf	Feb	1247	630	580	117	2401	952		1478	*Ohta and Okita,* [1990]
Sapporo, Japan	43 N	141 E	surf	Dec	1078	302	462	120	1767	552		790	*Ohta and Okita,* [1990]
Sapparo, Japan	43 N	141 E	surf	Jan	1191	322	447	156	2159	638		571	*Ohta and Okita,* [1990]
State College, Pennsylvania	41 N	78 W	surf	Jun-Aug	2810	2298		537	3837	3181		615	*Suh et al.* [1994]
Sweden	59 N	17 E	surf	Jan-Dec	840	691		845	1340	1840		647	*Hanssen et al.* [1990]
Tehachapi, California	35.2 N	118.4 W	surf	Dec-Feb	180	326	247	339	247	796	764	365	*Jacob et al.* [1986]
Veszprem, Hungary	47 N	18 E	surf	Jun-Aug	1533	3426	467	401	3350	5431		2122	*Meszaros et al.* [1997]
Veszprem, Hungary	47 N	18 E	surf	Dec-Feb	1809	1035	1712	1872	5628	3497		1213	*Meszaros et al.* [1997]
Xinlong	38 N	120 E	surf	Oct	1540	2001		683	2650	4398		1564	*Huebert et al.* [1988]
Remote Continental Sites													
Amazon	3 N	60 W	bl	Apr-May	81	18	58	1	92	36		340	*Talbon et al.* [1990]
Amazon	3 N	60 W	bl	Jul-Aug	125	17		1	300	34		299	*Talbon et al.* [1990]
Amazon	3 N	60 W	ft	Apr-May	11	9	11	<1	37	9		5	*Talbon et al.* [1990]
Amazon	3 N	60 W	ft	Jul-Aug	20	12		<1	60	15		3	*Talbon et al.* [1990]
Arctic	55 N	160 W	bl	Jun-Aug	128	210	30	2	137	85		2	*Talbon et al.* [1990]
Arctic	55 N	160 W	ft	Jun-Aug	40	397	15	5	52	190		4	*Talbon et al.* [1990]
Arctic	65 N	160 W	bl	Jun-Aug	29	317	11	2	53	161		5	*Talbon et al.* [1990]
Arctic	65 N	160 W	ft	Jun-Aug	65	403	22	7	75	189		4	*Talbon et al.* [1990]
Congo	4 N	14 E	surf	Jun	216	89	447	69	902	236		1594	*Clairac et al.* [1988]
Congo	4 N	14 E	surf	Oct	268	29	70	133	533	175		1593	*Clairac et al.* [1988]
Guyana	4 N	58 W	surf	Jun	65	25	5	<1	154	44		256	*Gregory et al.* [1986]
Guyana	4 N	58 W	ft	Jun	26	9	2	<1	12	12		4	*Gregory et al.* [1986]
Niwot Ridge, Colorado	40.05 N	105.6 W	surf	Jan-Dec	113	440	224	211	259	764	236	261	*Langford et al.* [1992]
Niwot Ridge, Colorado	40.05 N	105.6 W	surf	Dec-Feb	90	241	22	369	202	606	135	106	*Langford et al.* [1992]
South Pole	-90 N	10 E	surf	Dec	32	28	3	2	70	25	19	<1	*Gras,* [1983]
Wright Valley	77 S	162 E	surf	Nov-Dec	50	28	23	1	58	13	13	1	*Gras,* [1983]
Yakutsk	62 N	130 E	surf	Jan-Dec	100	330		84	165	395		89	*Ohta et al.* [1992]
Marine Sites													
Atlantic	10 N	60 W	surf	Jun	10	25		<1	14	45		67	*Talbot et al.* [1986]

Table 7. (Continued)

Location	Latitude	Longitude	Altitude	Time	SO_4^{2-}		NO_3^-		NH_4^+		NH_3		Reference
					Obs	Sim	Obs	Sim	Obs	Sim	Obs	Sim	
Atlantic	28 N	60 W	surf	Jun	34	143		<1	60	150		36	*Talbot et al.* [1986]
Atlantic	32 N	31 W	surf	Apr-May	425	248		1	385	284		114	*Church et al.* [1991]
Atlantic	35 N	70 W	ft	Jan	100	119	89	1	135	81		5	*Whelpdale et al.* [1987]
Atlantic	37 N	25 W	bl	Jun	1260	152	716	1	1302	119		13	*Huebert et al.* [1996]
Atlantic	37 N	25 W	ft	Jun	393	292	382	<1	470	133		5	*Huebert et al.* [1996]
Atlantic	40 N	70 W	bl	Jan	124	428	166	457	1000	1064		263	*Whelpdale et al.* [1987]
Atlantic	45 N	55 W	surf	Apr-May	410	439		12	380	319		33	*Church et al.* [1991]
Bonin Island	27 N	142 E	surf	Nov-Dec	484	268	257	<1	750	219		39	*Yoshizumi and Asakuno,* [1986]
Pacific	2 N	170 E	surf	Apr-May	100	17		<1	140	33		192	*Quinn et al.* [1990]
Pacific	5 S	155 W	surf	Feb-Mar	160	48		<1	100	89		179	*Clarke and Porter,* [1993]
Pacific	5 N	155 W	surf	Feb-Mar	175	26		<1	130	50		187	*Clarke and Porter,* [1993]
Pacific	15 N	155 W	surf	Feb-Mar	125	51		<1	25	85		128	*Clarke and Porter,* [1993]
Pacific	23 N	170 E	surf	Apr-May	450	86		<1	130	152		59	*Quinn et al.* [1990]
Pacific	43 N	170 E	surf	Apr-May	325	575		19	400	570		173	*Quinn et al.* [1990]
Pacific	46 N	126 W	bl	May	60	553		1	75	314		15	*Andreae et al.* [1988]
Pacific	50 S	160 W	surf	Mar-May	250	57	96	<1	115	25		4	*Parungo et al.* [1986]
Pacific - Hawaii	20 N	160 W	surf	Mar-May	250	127		<1	115	156		43	*Parungo et al.* [1986]
Santa Maria island	37 N	25 W	surf	Jun	475	166	311	<1	461	160	200	30	*Huebert et al.* [1996]
Tasmania	43 S	144 E	surf	Dec	40	68	9	1	70	134		219	*Berresheim et al.* [1990]
West Atlantic	31 N	75 W	surf	Jan-Dec	828	293	289	1	1206	289		79	*Berresheim et al.* [1990]

Mixing ratios are in parts per trillion by volume.
* Abbreviations are bl, boundary layer; ft, free troposphere; surf, surface.

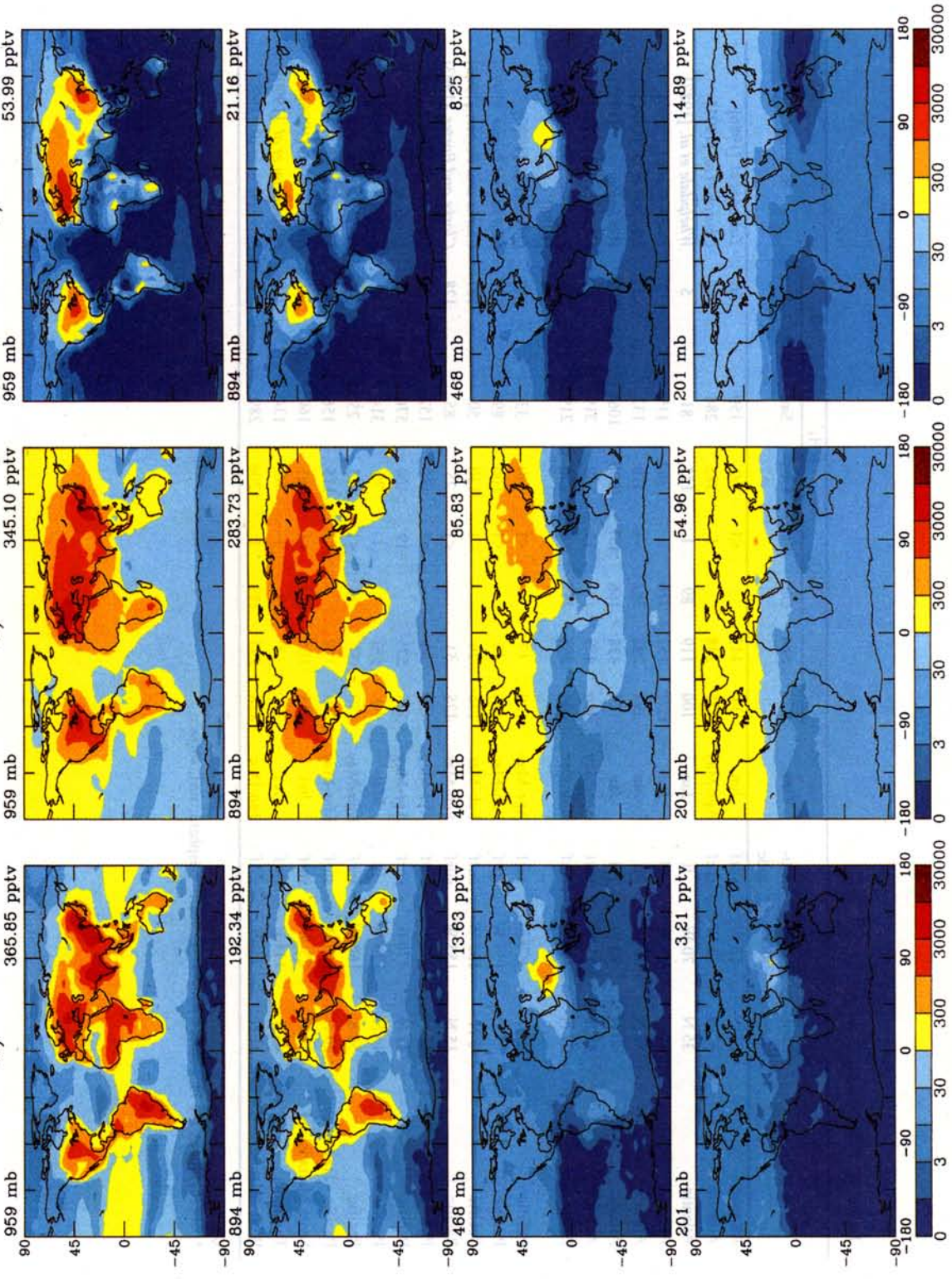

Plate 3. (a) Annual average ammonia mixing ratios. Note that 1 μg m^{-3} NH_3 = 1457 pptv NH_3 at 298 K and 1 bar. (b) Annual average ammonium mixing ratios. Note that 1 μg m^{-3} NH_4^+ = 1377 pptv NH_4^+ at 298 K and 1 bar. (c) Annual average nitrate mixing ratios. Note that 1 μg m^{-3} NO_3^- = 400 pptv NO_3^- at 298 K and 1 bar. Above each plot, the pressure level of the corresponding model layer is indicated, as is the average mixing ratio in that layer. Contour lines are 1, 3, 10, 30, 100, 300, 1000, 3000, 10,000, and 30,000 pptv.

13,808 ADAMS ET AL.: GLOBAL AEROSOL CONCENTRATIONS IN GCM

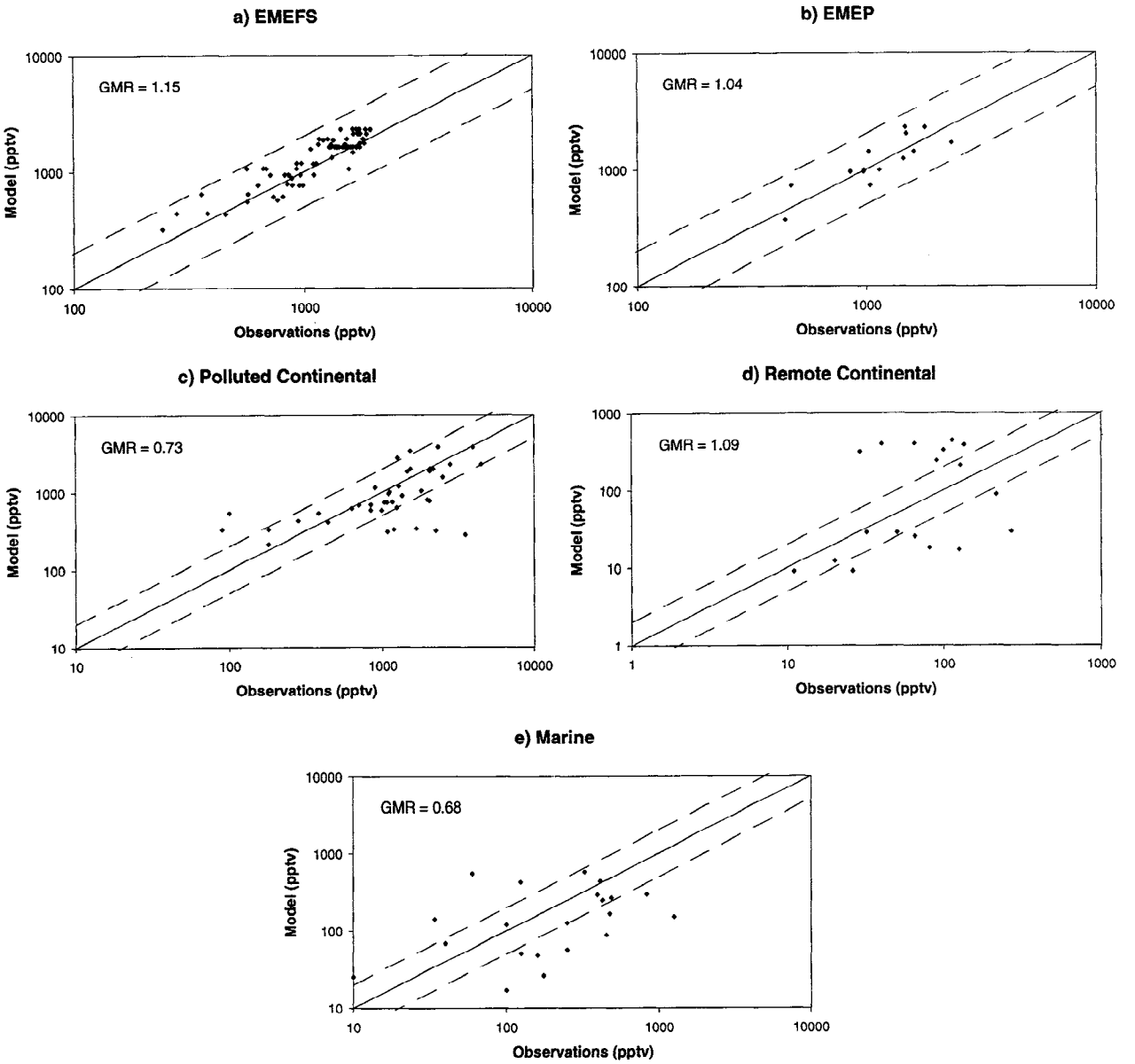

Figure 2. Scatterplot of simulated sulfate mixing ratios versus observations from (a) the EMEFS database, (b) the EMEP database, (c) polluted continental areas, (d) remote continental areas, and (e) marine areas. Dashed lines indicate 2:1 and 1:2 ratios. The geometric mean over all the ratios of simulated to observed mixing ratios (GMR) is indicated.

1994]. Gas phase ammonia has a steeper vertical gradient than ammonium because ammonia partitions preferentially into the particle phase. High concentrations of gas phase NH_3 exist only in polluted areas near the surface, where ammonia emissions exceed the capacity of the sulfate aerosol to absorb them. As the stoichiometric balance between ammonia and sulfate shifts toward sulfate higher in the atmosphere, a larger fraction of the total ammonia partitions into the aerosol phase.

Ammonium concentrations calculated here are similar to those of DC94, including locations and magnitudes of the peak ammonium levels in China, Europe, North America, and South Africa and the pattern of oceanic ammonium concentrations. More discrepancies can be found when comparing ammonia concentrations. While similar peaks in ammonia concentrations are found over India, we predict maxima over China, Europe, North America, and Brazil, not found in DC94. This difference can be explained by a combination of higher ammonia emissions and a slightly lower sulfate burden. The sulfate burden in this model, 0.73 Tg S, is just slightly lower than that reported by *Langner and Rodhe* [1991], 0.77 Tg S, upon which the sulfate component of DC94

Table 8. Geometric mean ratios of simulated to observed values for each species and observational database.

Species	EMEFS	EMEP	Pol. Cont.	Rem. Cont.	Marine
SO_4^{2-}	1.15	1.04	0.73	1.09	0.68
NO_3^-	2.29	1.50	0.51	0.14	
NH_4^+	1.23	1.63	0.84	0.74	0.75
NH_3	1.95		0.94	0.28	

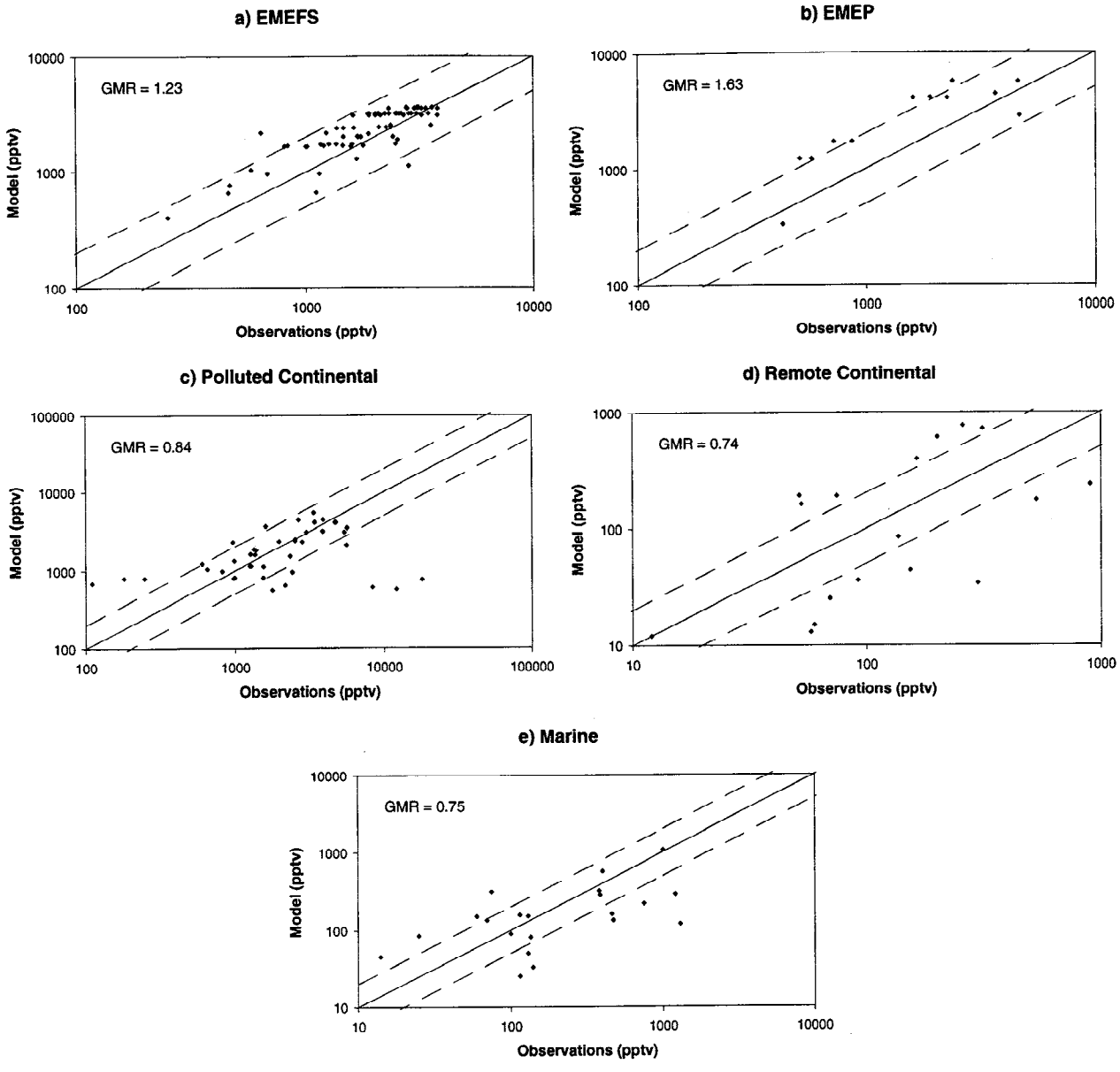

Figure 3. Scatterplot of simulated ammonium mixing ratios versus observations taken from (a) the EMEFS database, (b) the EMEP database, (c) polluted continental areas, (d) remote continental areas, and (e) marine areas. Dashed lines indicate 2:1 and 1:2 ratios. The geometric mean over all the ratios of simulated to observed mixing ratios (GMR) is indicated.

is based. The updated ammonia emissions inventory used here, however, is about 20% higher than that used by DC94. The combination of higher ammonia emissions and lower sulfate burden results in significantly higher gas phase ammonia concentrations in areas, such as those mentioned above, where the sulfate aerosol is nearly fully neutralized. Also, the coarse horizontal resolution of the model used by DC94 may have limited their ability to resolve some of these maxima. Oceanic ammonia concentrations, on the other hand, tend to be lower than those found in DC94.

Figure 3 shows scatter plots of simulated versus observed ammonium mixing ratios for the databases described above. It can be seen that predictions are within a factor of 2 of most observed ammonium mixing ratios. Comparison of simulated mixing ratios with the EMEFS database is especially close. This agreement is significant because the EMEFS database offers the highest quality observations, from the standpoint of both number of sites and length of sampling period. This suggests that some of the scatter in comparisons with other data sets may be a result of subgrid variability, interannual variability, short sampling times, or other sources of variability that one would not expect the GCM to resolve. Table 8 shows that the geometric mean ratios for ammonium are within about 25% of unity for all but the EMEP data set. Considering that the uncertainty in the ammonia emissions inventory is estimated to be 25% on a global scale and larger on a regional scale, one cannot expect better predictions without also evaluating the emissions inventory itself. Furthermore, Table 8 shows that some of the ammonium overprediction in North America and underprediction of

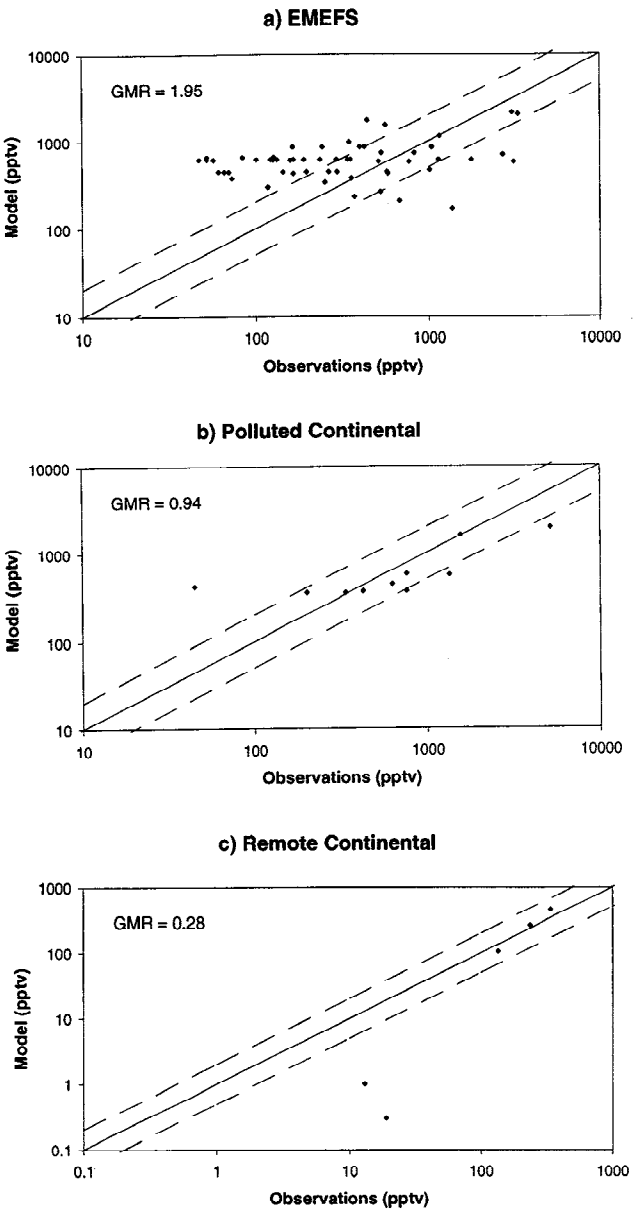

Figure 4. Scatterplot of simulated ammonia mixing ratios versus observations taken from (a) the EMEFS database, (b) polluted continental areas, and (c) remote continental areas. Dashed lines indicate 2:1 and 1:2 ratios. The geometric mean over all the ratios of simulated to observed mixing ratios (GMR) is indicated.

ammonium in the polluted continental and marine data sets must be ascribed to corresponding deviations in the sulfate fields. Predicted ammonium mixing ratios for Europe, on the other hand, seem distinctly high, although some allowance has to be made for the fact that the EMEP 1990 database represents fewer sites than the others. It is also worth noting that relative to sulfate, ammonium is overpredicted in all the data sets except the remote continental.

Excessive ammonium nitrate formation is one potential explanation for the high predicted ammonium levels in Europe. Ammonium overprediction is strongest in Europe, the area with the highest ammonium nitrate concentrations. As we will see later, simulated nitrate concentrations for Europe are also high compared with observations, further suggesting that ammonium nitrate in Europe is overestimated in the model.

Comparing predicted gas phase ammonia concentrations to observations is more problematic than doing so for ammonium. Fewer data are available, and risk of contamination [*Quinn et al.*, 1987] makes sampling gas phase ammonia much more difficult. Since ammonia partitions preferentially into the particle phase, errors in modeling sulfate and ammonium tend to compound ammonia modeling errors. If total ammonium and sulfate concentrations are roughly in balance, a small overprediction of sulfate or a low estimate of ammonia emissions will dramatically lower the predicted concentration of gas phase ammonia, and vice versa. Finally, the lifetime of gas phase ammonia is significantly shorter than those of sulfate and ammonium, so even stronger concentration gradients exist. Figure 4 shows scatter plots of how simulated ammonia mixing ratios compare with observations taken from EMEFS and the literature. No scatter plots are shown for the EMEP and marine databases, since they represent only four sites between them.

Roughly 40% of the simulated ammonia mixing ratios are within a factor of 2 of the literature observations, and the geometric mean ratio of 1.95 for the comparison indicates a significant high bias in the simulated values. While many of the simulated ammonia mixing ratios compare well with the EMEFS database, the GCM simulation does not seem to exhibit as much variability as the observational data. In particular, predicted ammonia mixing ratios uniformly exceed observations at a number of sites. A close examination of the EMEFS database, however, demonstrates that much of the variability in observed ammonia concentrations occurs on spatial scales that the GCM cannot resolve. The three GCM grid cells with the most sites had 16, 8, and 6 EMEFS observational sites. Observed ammonia mixing ratios in these grid cells ranged from 47 to 1782 pptv, 61 to 574 pptv, and 164 to 1044 pptv, respectively; thus observed ammonia mixing ratios varied by an order of magnitude or more on the subgrid scale. Predicted ammonia mixing ratios for these three cells were 612, 442, and 854 pptv, which are within the respective ranges of observed values.

Figure 5 shows the annual average ammonia budget for the global troposphere. Nearly half of the 53.6 Tg N of ammonia emitted each year is taken up by the aerosol phase. As a result, the deposition flux of gas phase ammonia is almost exactly the same as that of particulate ammonium. However, 72% of NH_3 total deposition is dry, while 75% of NH_4^+ deposition is wet. Only 1.1 Tg N yr^{-1} of ammonia, about 2% of emissions, undergoes reaction with the OH radical. This is lower than the value of DC94, 1.8 Tg N yr^{-1} because of the current lower ammonia burden. As expected, the lifetime of particulate ammonium, 4.2 days, is longer than that of gas phase ammonia, 1 day. The lifetime of NH_x (NH_3 + NH_4^+) is 3 days. The NH_4^+ lifetime is similar to that calculated by DC94, 4.5 days. On the other hand, the DC94 ammonia lifetime, 2.1 days, is significantly longer than that predicted here. Our lifetimes with respect to ammonium formation and wet deposition are both about half of those implied by the budget figures of DC94, while the lifetime of NH_3 with respect to dry deposition is one third of the corresponding value in DC94. Dry deposition, wet deposition, and gas-to-particle conversion therefore all contribute to the lower NH_3 lifetime in our model, with the contribution of dry deposition being somewhat more

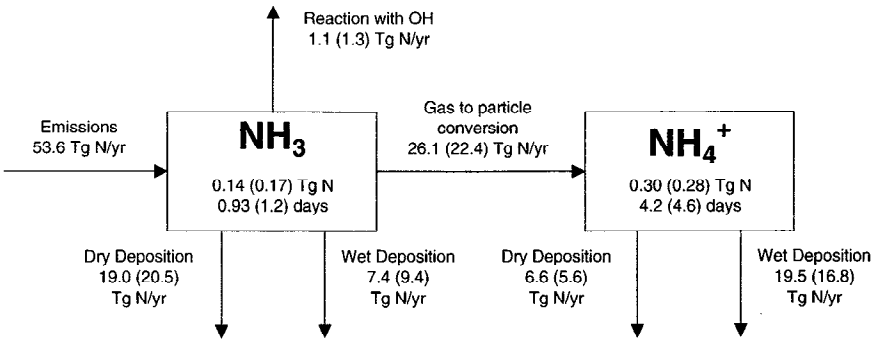

Figure 5. Global and annual average ammonia budget. Arrows indicate net fluxes. Burdens and lifetimes of ammonia and ammonium are shown in their respective boxes. Values inside parentheses are taken from a sensitivity study in which nitric acid is neglected.

important. DC94 used a canopy compensation point concept to model emission from and dry deposition to the soil-vegetation complex, and this difference in accounting means our budget figures are not directly comparable. Other differences in dry deposition between the two models could result from different surface layer thicknesses as well as differing ways in which the respective models estimate the aerodynamic resistance to dry deposition. DC94 used a parameterized treatment of wet deposition based on a climatology of precipitation rates, which can be expected to lead to very different results from the GCM treatment of precipitation and wet deposition used here. Finally, DC94 limited ammonia uptake by sulfate aerosols to a point where the molar ratio of ammonium to sulfate was 1.5. We allow neutralization of sulfate (and nitrate) to occur according to thermodynamic equilibrium. Later, we show that the aerosol is almost completely neutralized in many regions with high ammonia emissions. This additional uptake of ammonia, beyond that allowed by DC94, also contributes substantially to the shorter lifetime of ammonia in our model.

As a result of the longer lifetime of NH_4^+ than NH_3, on an annual average basis, there is about twice as much particulate NH_4^+ as gas phase NH_3. The calculated burden of NH_4^+ is 0.30 Tg N, while that of NH_3 is 0.14 Tg N. DC94 report a similar NH_4^+ burden, 0.33 Tg N, but their NH_3 burden is nearly twice as large, 0.26 Tg N. The reasons for the discrepancy in NH_3 burden are the same as those discussed in regard to the difference in NH_3 lifetimes. As a final note, comparing the values for the standard model run with those from the sensitivity run with zero nitric acid, shown in parentheses in Figure 5, demonstrates that the formation of NH_4NO_3 aerosol has a modest effect on the overall ammonia budget by converting an additional 3.7 Tg N yr^{-1} of ammonia to ammonium.

3.4. Nitrate

Annual average mixing ratios of nitrate aerosol are shown in Plate 3c. We predict a large area of significant nitrate aerosol formation in Europe, with smaller areas in China and the eastern United States. Nitrate mixing ratios exceed 1 ppbv (1 $\mu g\ m^{-3}\ NO_3^-$ = 400 pptv NO_3^- at 298 K and 1 bar) in these regions. Most continental areas in the Northern Hemisphere have nitrate mixing ratios exceeding 100 pptv. In the Southern Hemisphere, this is only true in highly localized areas, such as parts of South America and South Africa. Marine mixing ratios of nitrate aerosol are negligible (less than 1 pptv) nearly everywhere. Nitrate concentrations decrease rapidly up to the middle troposphere but show a modest increase in the upper troposphere and lower stratosphere. This increase results from higher HNO_3 concentrations near the tropopause, as well as an increased solubility of HNO_3 in the aerosol phase at lower temperatures.

Two different types of aerosol nitrate formation occur. At midlatitudes and near the surface, where temperatures are warmer, thermodynamic considerations require that aerosol nitrate occur only as neutralized ammonium nitrate. Nitrate formation in developed areas therefore is enhanced by available ammonia and reduced by the presence of sulfate, which reacts preferentially with ammonia. In colder areas near the poles and in the upper troposphere, the solubility of nitric acid in water is high, and aerosol nitrate occurs here despite the lack of available ammonia to neutralize it. Sulfate enhances the formation of aerosol nitrate in cold areas by providing the aerosol water that solvates the nitric acid.

For several reasons, comparing simulated nitrate concentrations to observed values is also problematic. First, there are fewer observations of nitrate than of sulfate and ammonium. Second, as described above, there is uncertainty in the HNO_3 fields taken as input for this model, especially in remote areas. Another potential problem is that particulate nitrate may evaporate from filter packs, and the resulting measurements may be biased by as much as 24% [*Pakkanen et al.*, 1999]. Finally, formation of nitrate aerosol in the boundary layer depends on the availability of excess ammonia beyond that required to neutralize sulfate. As a result, nitrate concentrations in the model can be sensitive to small errors in predicted ammonia concentrations. Comparisons of predicted and observed annual average nitrate mixing ratios are shown in Figure 6. Most of the model predictions are within a factor of 2 of the EMEP observations. We seem to overpredict nitrate aerosol in Europe, although this is difficult to assess based on the few observations available. In North America, predictions match observations at many locations but tend to overestimate at sites with low levels of observed nitrate. The most serious discrepancy between simulated nitrate mixing ratios and observations occurs at marine locations. Here the model predicts nitrate mixing ratios of about 1 pptv or less, while mixing ratios of 50-500 pptv are typically observed. This is attributed to the absence in the model of sea salt upon which nitric acid is known to condense. Predictions seem too low

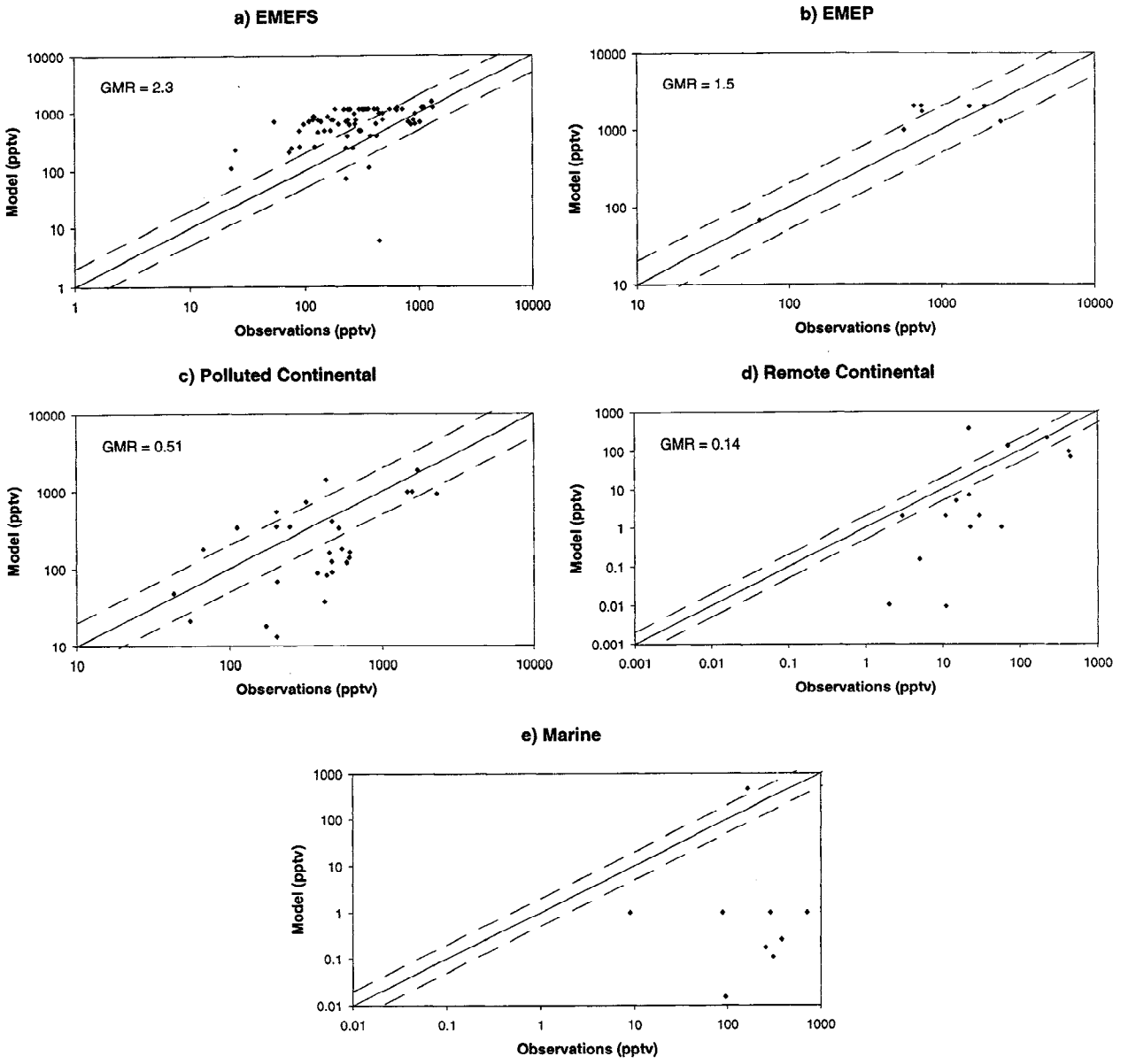

Figure 6. Scatterplot of simulated nitrate mixing ratios versus observations taken from (a) the EMEFS database, (b) the EMEP database, (c) polluted continental areas, (d) remote continental areas, and (e) marine areas. Dashed lines indicate 2:1 and 1:2 ratios. The geometric mean over all the ratios of simulated to observed mixing ratios (GMR) is indicated.

when compared with observations of nitrate in polluted and remote continental areas, but it is difficult to draw any meaningful conclusions from a comparison between GCM output and short-term observations.

Besides the absolute concentration of nitrate aerosol, it is also interesting to examine the partitioning of total nitrate, gas and aerosol, between the two phases. Plate 4a shows the percent of total nitrate occurring in the aerosol phase. We note that throughout most areas of the atmosphere, less than 10% of total nitrate is in the aerosol phase. However, the availability of excess ammonia, beyond that which is necessary to neutralize sulfate, drastically changes this situation in key areas. More than half of total nitrate is found in the aerosol phase in eastern Asia, across a broad area of Europe and into western Russia, as well as in the North American Midwest. In contrast, nitrate does not partition as strongly into the particle phase in other areas with similarly high gas phase ammonia concentrations, such as Brazil, India, and equatorial Africa, where warmer temperatures make gaseous nitric acid thermodynamically more favorable. At least 10% of total nitrate is found in the aerosol phase throughout most continental areas in the northern midlatitudes. The only marine areas where more than 10% of nitrate is found in the aerosol phase are polar regions, where HNO_3 is soluble in aerosol water because of the cold temperatures. Partitioning of HNO_3 into the aerosol phase decreases with altitude up through the lower to middle troposphere because of a lack of free ammonia, but increases again in the upper troposphere because of the enhanced solubility of nitric acid in aerosol water at colder

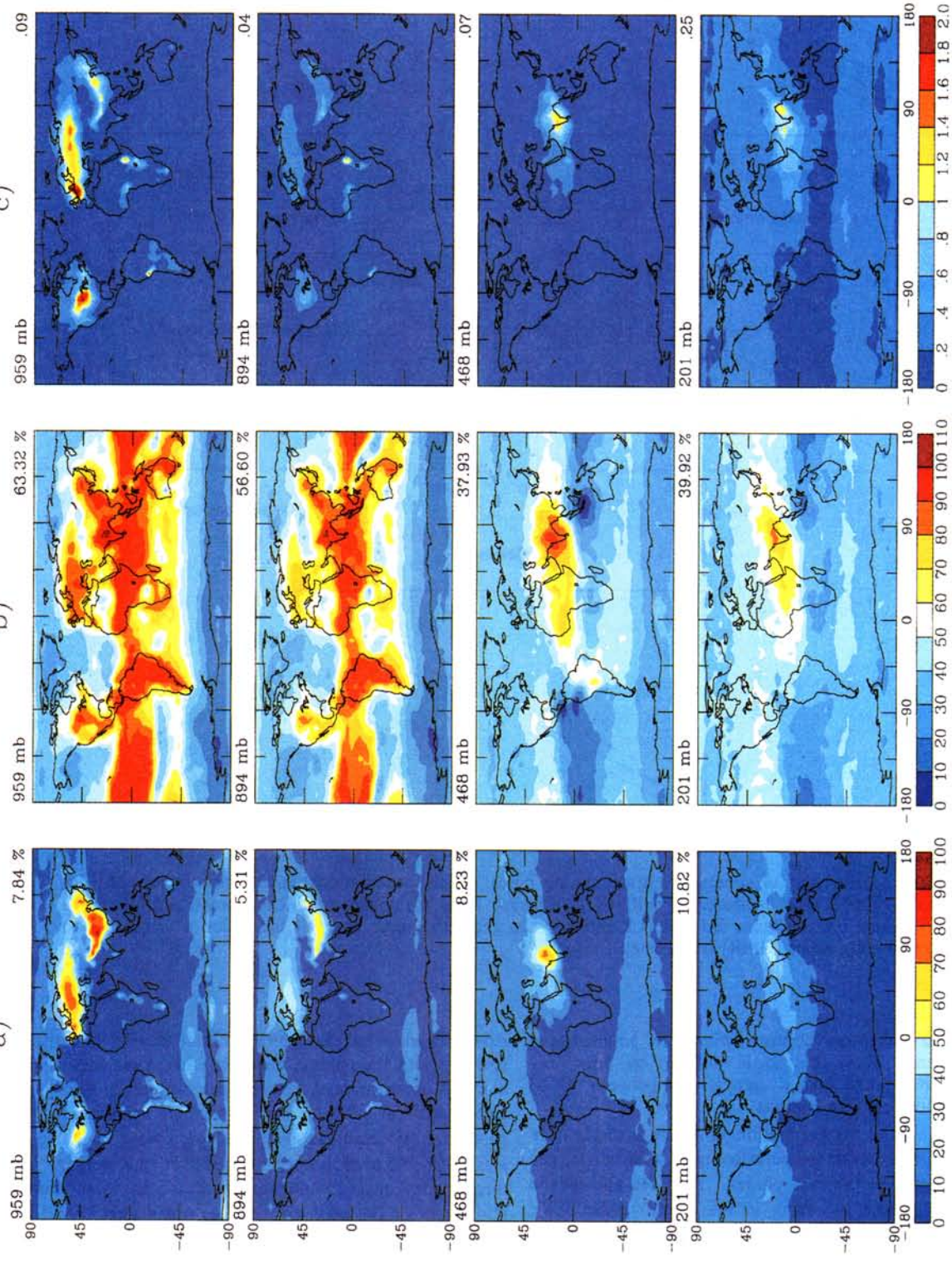

Plate 4. (a) Percent of total HNO_3 occurring in the aerosol phase. (b) Percent of acidic anions (sulfate and nitrate) neutralized by aerosol ammonium (See definition of DON in text). (c) Nitrate to sulfate molar ratios. Above each plot, the pressure level of the corresponding model layer is indicated, as is the average value for that layer.

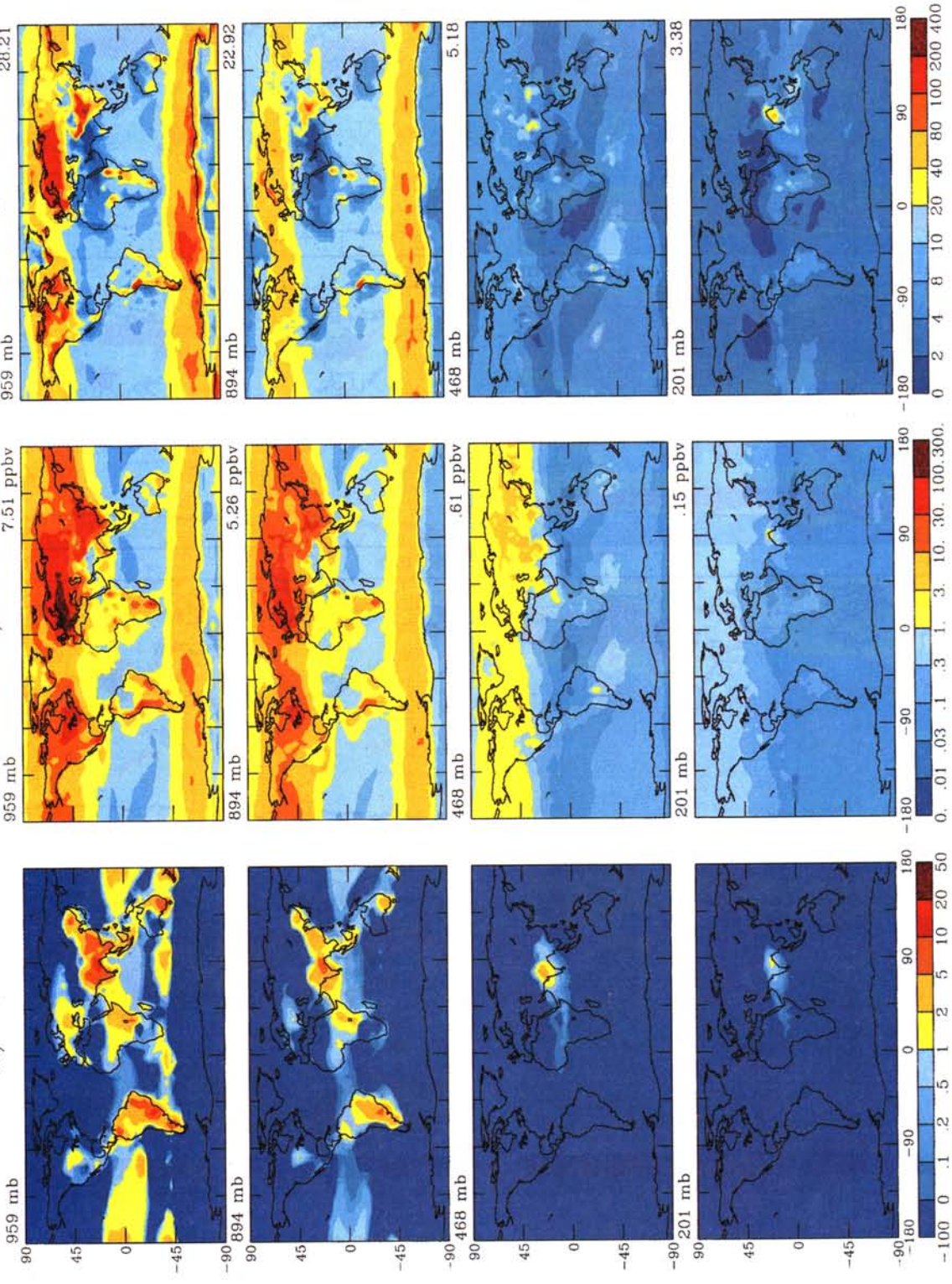

Plate 5. (a) The gas ratio (defined in text). (b) Annual average aerosol water mixing ratios. (c) Aerosol water to sulfate molar ratios. Above each plot, the pressure level of the corresponding model layer is indicated as well as average values for Plates 5b and 5c.

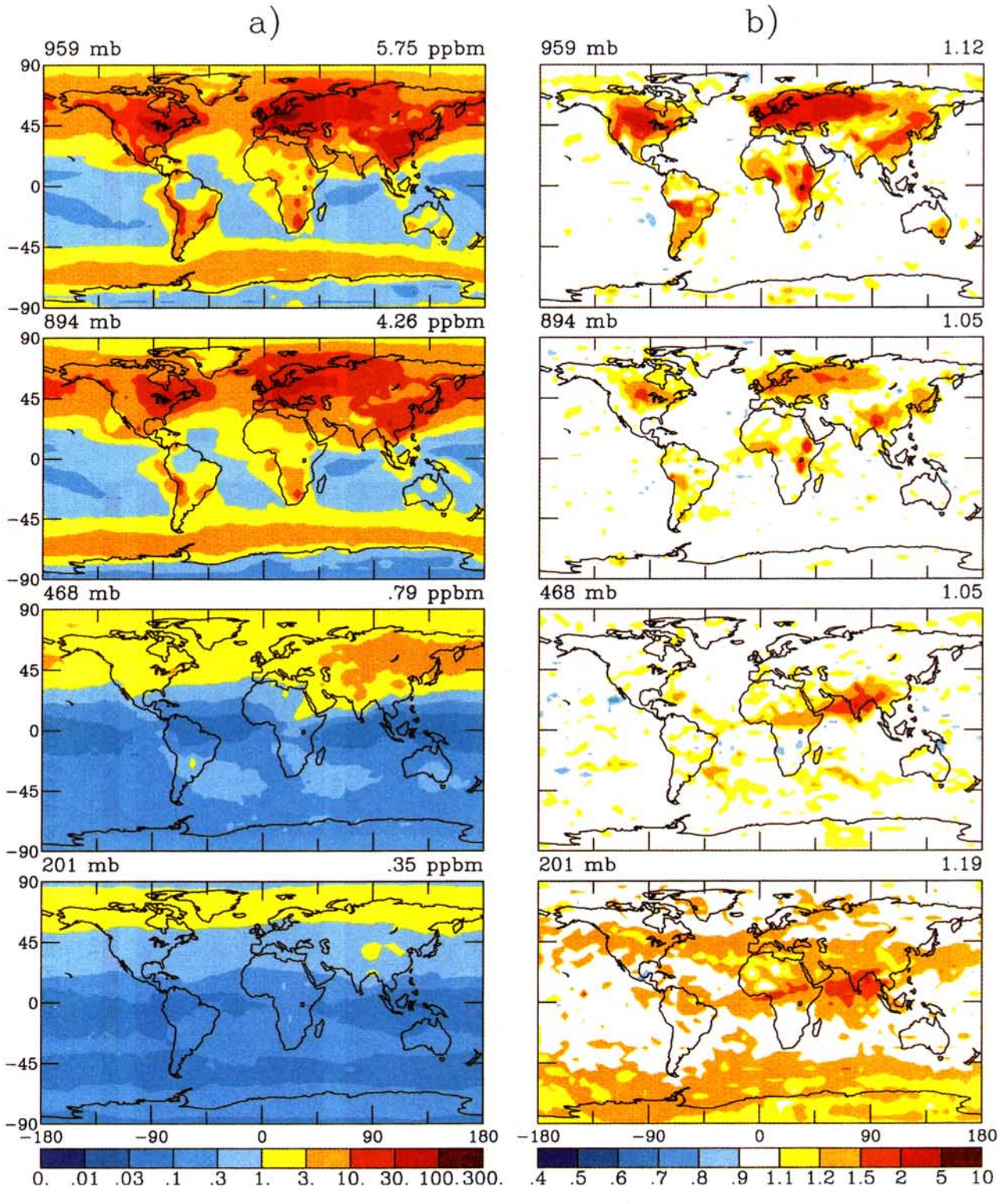

Plate 6. (a) Annual average aerosol mass mixing ratios. (b) Nitrate enhancement of total aerosol mass (ratio of annual average aerosol mass to that assuming no HNO_3). Above each plot, the pressure level of the corresponding model layer is indicated, as is the average value for that layer.

temperatures. The only exception to this behavior is India, where less than 10% of nitric acid occurs as aerosol in the model surface layer but over 50% occurs as aerosol at around 400 mbar. This can also be explained in terms of free NH_3 and temperature. High concentrations of free NH_3 exist near the surface in India, but warm temperatures prevent the formation of nitrate aerosol. In the colder middle troposphere the area above India is the only region with sufficiently high concentrations of free NH_3 for nitrate formation.

3.5. Interactions Among Species

Having calculated global concentration fields for sulfate, nitrate, and ammonium, we would like to explore to what degree the acidic aerosol species, sulfate and nitrate, are neutralized by particulate ammonium. We define degree of neutralization (DON) as the equivalents of basic species divided by the equivalents of acidic species,

$$\mathrm{DON} = \frac{\left[\mathrm{NH_4^+}\right]}{2\left[\mathrm{SO_4^{2-}}\right] + \left[\mathrm{NO_3^-}\right]} \tag{4}$$

The degree of neutralization is analogous to the ammonium-sulfate molar ratio for a system without nitrate. A neutralization of 100% indicates that all sulfate and nitrate exist as ammonium sulfate and ammonium nitrate, respectively. A lower neutralization indicates a more acidic aerosol. Note that ammonium, sulfate, and nitrate are not the only particulate species that contribute to the pH of the aerosol phase. For example, formic and acetic acids are sometimes the dominant sources of acidity in precipitation in remote areas [*Talbot et al.*, 1992; *Seinfeld and Pandis*, 1998], so the degree of neutralization does not exactly correspond to pH. The degree of neutralization of the global aerosol is shown in Plate 4b. Near the surface, the results show a high degree of spatial variability with a pattern that does not neatly correspond to a typical division among industrialized, remote continental, and marine areas. Values of the degree of neutralization range from a low around 10% for Antarctica to completely neutralized for large regions of the globe centered around the equator. This pattern of aerosol neutralization could not be captured except in a three-dimensional transport model with an aerosol thermodynamic calculation.

Aerosols in the continental areas with the highest ammonia emissions, China, India, eastern Europe, and central North America, are all nearly completely neutralized. For the most part, areas with high ammonia emissions, usually a product of intense agricultural activity, generally correspond to industrialized areas that have high sulfate concentrations. The aerosol in industrialized areas of Europe and China therefore tends to be neutralized. This is not the case in the eastern United States where ammonia emissions are not sufficient in magnitude, and occur somewhat too far westward, to completely neutralize the aerosol here. In some remote continental areas, such as South America and equatorial Africa, the aerosol is completely neutralized, while in other areas, such as Siberia, the aerosol is less than half neutralized. The large amount of excess NH_3 over India produces an interesting result. Here there is a small area with a "neutralization" that exceeds 100%, indicating that NH_3 concentrations are sufficiently high not only to neutralize the sulfate and nitrate, but also to force an extra amount of ammonia into the aerosol phase via Henry's law solubility.

The degree of neutralization over the oceans reflects the balance between DMS and ammonia emissions. The pattern of the oceanic gyres can be seen in Plate 4b, with the aerosol in the more biologically active gyres tending to be neutralized to a greater degree than that found in the central oceans. While this result is highly uncertain because of the large uncertainties associated with oceanic emissions, it seems to be consistent with the observations found in Table 7.

Despite considerable variability of the degree of aerosol neutralization within both continental and marine areas, it is worth pointing out that, on average, continental aerosol is more neutralized than marine. The model predicts this result, which is consistent with observations, because of its realistic thermodynamic treatment of gas-aerosol partitioning.

A final observation is that the degree of neutralization of the aerosol decreases with altitude. This is expected because sulfate and nitrate are both produced via gas phase and heterogeneous chemistry at all levels of the atmosphere, whereas ammonia is emitted at the surface and has no sources above the surface. As a result, upper tropospheric aerosol tends to be more acidic than that at the surface. The decrease in the degree of neutralization, however, is not drastic, from an average of 63% near the surface to 40% at the tropopause.

In order to make a general assessment of the relative importance of nitrate as an aerosol constituent, Plate 4c shows the global molar ratio of aerosol nitrate to sulfate. Over most of the globe, molar concentrations of nitrate aerosol are small compared with those of sulfate (the average value is less than 10%), but nitrate is regionally important in eastern Asia, Eurasia, and the North American Midwest. In these areas, there is as much nitrate as sulfate on a molar basis. These nitrate "hotspots" disappear rapidly with altitude; even in the second model layer near 900 mbar, these are only faint echoes of their surface values. In the upper troposphere and lower stratosphere, nitrate becomes significant once again. Here, however, instead of localized areas of extreme importance, nitrate has a more modest importance across a much larger area.

With respect to gas-aerosol sulfate-nitrate-ammonia equilibrium, *Ansari and Pandis* [1998] have defined the gas ratio (GR) as

$$\mathrm{GR} = \frac{\left[\mathrm{NH_3^F}\right]}{\left[\mathrm{HNO_3^T}\right]} = \frac{\left[\mathrm{NH_3^T}\right] - 2\left[\mathrm{SO_4^{2-}}\right]}{\left[\mathrm{HNO_3^T}\right]} \tag{5}$$

where $[HNO_3^T]$ is the total (gas plus aerosol) nitric acid concentration, $[NH_3^T]$ is the total (gas plus aerosol) ammonia concentration, and $[SO_4^{2-}]$ is the sulfate concentration. Free ammonia, $[NH_3^F]$, is the amount of ammonia available, after neutralizing sulfate, for ammonium nitrate formation. The significance of the gas ratio is that it indicates which reactant, ammonia or nitric acid, limits the formation of ammonium nitrate. A gas ratio that is greater than 1 indicates that nitric acid is limiting, while a ratio between 0 and 1 indicates that while some ammonia is available for reaction with nitric acid, ammonia is limiting. A gas ratio that is less than 0 indicates that ammonia is severely limiting. In this case, formation of ammonium nitrate is impossible because all ammonia will first react with sulfate.

Plate 5a shows the global gas ratio computed from annual average concentrations. On an annual average basis, throughout most of the atmosphere, there is no free ammonia, so ammonium nitrate formation generally does not occur. Note

that even in locations where the gas ratio, based on annual average concentrations, is less than zero, free ammonia may exist during certain parts of the year, and ammonium nitrate formation can occur during those times.

However, free NH_3 exists on a regular basis in many of the most populated areas of the globe. Ammonium nitrate formation in the areas with the highest nitrate concentrations, Europe, China, and the American Midwest, is generally limited by HNO_3 concentrations. It is not surprising to see that other areas with high ammonia NH_3, such as Brazil and India, have high gas ratios. The concentrations of ammonium nitrate in these areas could increase dramatically given an increase in HNO_3 concentrations. On the other hand, ammonia tends to be limiting in remote continental and marine areas. The gas ratio decreases with altitude because, for reasons discussed above, the concentrations of total ammonia decrease more rapidly than those of sulfate.

3.6. Aerosol Water

Annual average mixing ratios of aerosol water are shown in Plate 5b. Broadly speaking, there are no major surprises in this picture. Aerosol water mixing ratios are usually highest in industrialized areas with high sulfate concentrations, reaching values greater than 100 ppbv in Europe. Aerosol water mixing ratios in continental areas are greater than 1 ppbv almost everywhere. Low mixing ratios of aerosol water, 100 to 300 pptv, are found in the areas of lowest sulfate concentrations, the remote Pacific and Indian Oceans. Marine mixing ratios may be as high as 10 ppbv, however, in cold areas with high sulfate concentrations. It is clear from this figure that aerosol water content decreases rapidly with altitude, even more rapidly than sulfate concentrations. The average aerosol water mixing ratio at 200 mbar is 2% of the surface value. Obviously, relative humidity plays an important role here. A close comparison of aerosol water and sulfate concentrations shows that even in the lowest model layer, sulfate concentration is not the only parameter with a significant effect on aerosol water. Both relative humidity and presence of nitrate are also important.

The effects of relative humidity and nitrate level can be more clearly seen in Plate 5c. Plate 5c shows the molar ratio of water to sulfate, which varies by roughly 2 orders of magnitude as a result of water uptake by nitrate as well as the effects of relative humidity and degree of neutralization. For example, a region of very dry aerosol over the desert area extends from northwestern India, past Saudi Arabia, and through northern Africa. Aerosol transported from Europe to this dry area will be less effective at radiative forcing than aerosol that remains in more humid areas. The molar ratio of water to sulfate is apparently very high in Europe (greater than 100 mol of water per mole of sulfate), but this is mostly due to water uptake by aerosol nitrate. Finally, there is a small band of enhanced sulfate concentrations in the Southern Ocean between South America and Antarctica, which is mostly unneutralized. Plate 5c shows how this unneutralized sulfate is more efficient in taking up water than is neutralized sulfate. These results are important because most studies of radiative forcing due to sulfate aerosol have assumed a uniform water uptake per mole of sulfate. Although local variations in water uptake due to composition and relative humidity may not significantly alter global and annual average forcing, they can distinctly change its spatial distribution.

3.7. Aerosol Mass

Aerosol mass mixing ratio, the sum of all aerosol components considered here (sulfate, nitrate, ammonium, and aerosol water), is shown in Plate 6a. Highest aerosol mass mixing ratios predicted by the model occur in central Europe, where they exceed 100 ppbm, but mixing ratios exceed 30 ppbm over a much larger area as well as in China and around the Great Lakes in North America. Aerosol mass mixing ratios exceed 1 ppbm nearly everywhere in the Northern Hemisphere, whereas marine areas in the Southern Hemisphere generally exhibit mixing ratios less than 1 ppbm. It is interesting to note the band in the Southern Ocean around Antarctica where aerosol mixing ratios exceed 3 ppbm. Sulfate aerosol produced by oxidation of DMS in this region is highly acidic, being a mixture of sulfuric acid and ammonium bisulfate, which is especially hygroscopic at the colder temperatures found around Antarctica. The remote Pacific and Indian Oceans show the lowest aerosol mass mixing ratios, 100 to 300 pptm. As expected, aerosol concentrations quickly decrease with altitude and are about an order of magnitude lower at the tropopause than at the surface.

3.8. Seasonal Cycles

Seasonal cycles in sulfate concentrations, total nitric acid concentrations, ammonia emissions, temperature, and precipitation can all give rise to seasonal cycles in ammonia, ammonium, and nitrate concentrations. Here we examine the temporal behavior of the GCM predictions.

Figure 7 shows the seasonal cycles in simulated sulfate, nitrate, ammonium, and ammonia mixing ratios compared with observations at four EMEFS sites. In order to focus on the seasonal behavior of nitrate, ammonium, and ammonia, these sites were chosen because their simulated sulfate cycles closely resemble observations. In North America, sulfate concentrations typically peak during summer or early fall because higher OH and H_2O_2 concentrations in those months rapidly oxidize sulfur dioxide to sulfate. Since most ammonium is formed via uptake by sulfate aerosol, the observations show that ammonium concentrations tend to follow the same pattern of high summer concentrations. Formation of ammonium nitrate, on the other hand, is thermodynamically favored at lower temperatures, such that nitrate mixing ratios are 4-8 times higher during the winter at the sites shown here. Ammonia concentrations are low during the winter because emissions, which are primarily from agricultural activities, are also lowest then.

The most striking thing about the comparison of model behavior with observations is the nitrate concentrations, which are too high at the New York sites throughout the year and too high at the other sites during winter. The excessive amount of nitrate formation produces corresponding discrepancies in the ammonium concentrations. One explanation for the overestimation of NH_4NO_3 is that there is too much total ammonia, aerosol, and gas phase. The observations show that formation of NH_4NO_3 is suppressed during winter by the lack of free ammonia, as evidenced by the low gas phase NH_3 concentrations. In the model, on the other hand, gas phase NH_3 is too high throughout the year at Ithaca and Piseco, resulting in high nitrate concentrations. In fact, predicted concentrations of NH_3 tend to be highest during some of the winter months, allowing formation of ammonium nitrate. The model is therefore sensitive to the balance between

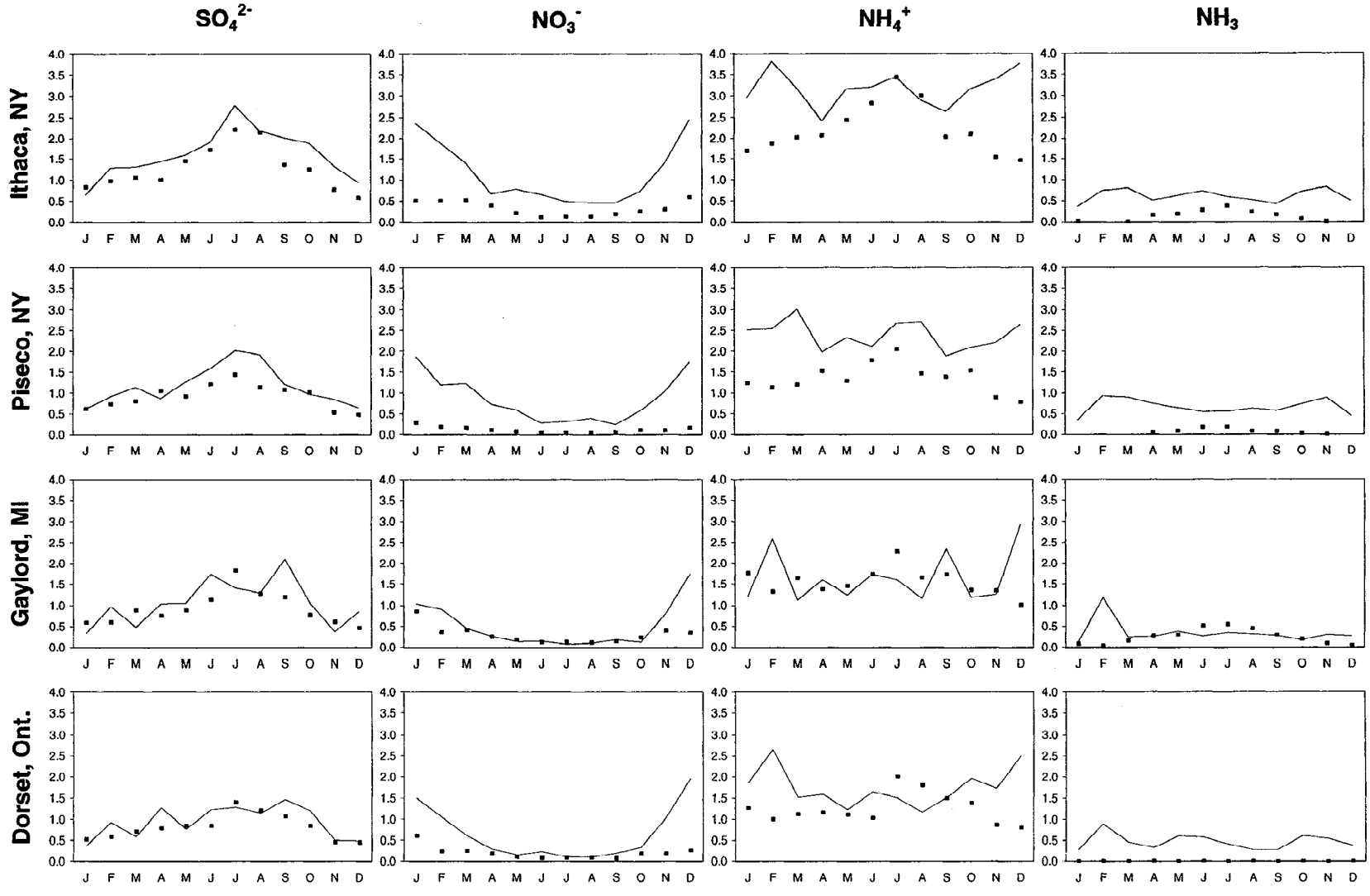

Figure 7. Comparison of simulated and observed seasonal cycles in the mixing ratios of model species at four EMEFS sites. Mixing ratios are monthly mean (ppbv). Solid lines indicate model values and squares indicate observed values.

ammonia and sulfate, and excess ammonia can dramatically increase nitrate concentrations.

4. Sensitivity Studies

To determine the effect of nitrate on total aerosol mass, a sensitivity study was performed in which the nitric acid concentration fields were set to zero. After generating annual average concentrations in the absence of nitrate, the total aerosol mass concentrations of this sensitivity study were compared with those of the base run. By comparing total aerosol mass, we see not only the additional mass of the nitrate ion itself, but also the mass of any accompanying ammonium and water. Plate 6b shows the ratio of total aerosol mass in the presence of nitric acid to that calculated in its absence. Because different runs do not identically reproduce all processes affecting tracer concentrations, a certain amount of noise is introduced into the comparison in the form of physically insignificant variability between runs. Although this noise is visible in the results, it is small in comparison with the effects we are examining.

Plate 6b shows that nitric acid has the most substantial effect on aerosol mass in and around the developed regions of the Northern Hemisphere. Accumulation mode nitrate formation does not substantially affect total aerosol mass in marine areas. In a large part of Europe and extending into Russia, aerosol mass concentrations in the model are more than double what they are in the absence of nitrate formation. The effect of nitric acid in eastern Asia is more modest, but still significant. Here, nitrate formation increases total aerosol mass between 50% and 100% in the most heavily influenced areas, and by at least 20% throughout the rest of the region. In the eastern United States the effect may be 20% to 50% or more, but HNO_3 affects central North America more strongly. In this area, with its high NH_3 emissions and relatively lower sulfate concentrations, ammonium nitrate formation is favored, and total aerosol mass more than doubles because of the presence of nitric acid. Since the particulate nitrate concentrations presented here seem to be higher than those observed, these estimates should be considered upper limits.

Another result to note is the influence of nitrate above India, where it is fairly unimportant near the surface, but has a more significant effect in the middle troposphere. In most other areas of the world, gas phase NH_3 mixing ratios exceed 1 ppbv only near the surface and in the boundary layer. Above India, however, the high ammonia emissions and relatively low sulfate concentrations result in significant amounts of gas phase NH_3 penetrating into the middle troposphere, allowing the formation of NH_4NO_3 aerosol at a higher altitude than anywhere else.

For reasons already mentioned above, nitrate formation is most important near the surface, where it increases total aerosol mass by 12% on average, and declines in importance to an average increase of 3% around 700 mbar. Nitrate importance increases again as one approaches the tropopause where it increases aerosol mass by 19%.

Total aerosol mass may be a nonlinear function of the availability of the various precursors: sulfur, nitric acid, and ammonia [*West et al.*, 1998]. For example, as sulfate concentrations decline, perhaps because of lower sulfur emissions, total aerosol mass may not decrease linearly if this decrease frees ammonia that is able to react to form ammonium nitrate. The GCM simulation allows us to examine the sensitivity of total aerosol mass to the availability of precursor species.

In a set of six sensitivity runs, we integrate the model through 1 year during which the availability of one of the three precursors, sulfur, ammonia, and nitric acid, is either increased or decreased by 25%. In the cases of sulfur or ammonia, this was accomplished by uniformly scaling global emissions. For nitric acid, the input concentration fields were changed by 25%. Table 9 shows the annual average global burden of the various aerosol species for the base run, the six sensitivity runs just described, as well as the sensitivity run without HNO_3.

In the standard scenario, the global burden of inorganic aerosol ions is 2.6 Tg. With 4.9 Tg of accompanying aerosol water, the total global aerosol burden is 7.5 Tg. Globally averaged, water makes up about two thirds of aerosol mass. The scenario without nitrate indicates that the total aerosol burden would be about 11% lower in the absence of nitric acid.

The six precursor sensitivity runs show that while total aerosol mass in certain regions of the globe may exhibit a nonlinear dependence on sulfate concentrations, most regions of the globe display a linear dependence on sulfate concentration. Nonlinear behavior is observed only in regions with substantial amounts of ammonium nitrate. As a

Table 9. Global and Annual Average Aerosol Burdens for Base Run and Sensitivity Cases

Species	No Nitrate	Base Run	S Emissions		[HNO_3]		NH_3 Emissions	
			-25%	+25%	-25%	+25%	-25%	+25%
			Aerosol Burden in Teragrams					
SO_4^{2-}	2.11	2.09	1.52	2.62	2.03	2.08	2.08	2.07
NO_3^-		0.13	0.15	0.11	0.1	0.15	0.09	0.17
NH_4^+	0.37	0.39	0.35	0.41	0.38	0.39	0.32	0.45
H_2O	4.23	4.88	3.85	5.89	4.68	4.97	4.85	4.9
Total	6.71	7.49	5.87	9.03	7.19	7.59	7.34	7.59
			Aerosol Burden as Percent of Base					
SO_4^{2-}	101	100	73	125	97	100	100	99
NO_3^-	0	100	115	85	77	115	69	131
NH_4^+	95	100	90	105	97	100	82	115
H_2O	87	100	79	121	96	102	99	100
Total	90	100	78	121	96	101	98	101

result, the global aerosol burden responds nearly linearly with changes in sulfur emissions and is insensitive to changes in ammonia emissions or nitric acid concentrations.

Changes in sulfate concentrations are virtually linear with changes in sulfur emissions. Although changes in nitrate concentrations do partly compensate for changes in sulfate concentrations, this has a small effect on the global burden. As for ammonium concentrations and water content, these are more affected by sulfate than nitrate, so they decrease when sulfate decreases, and vice versa. The net result is that the total aerosol burden changes by about 20% for a 25% change in sulfur emissions. However, in areas where nitrate formation is important, such as Europe as well as parts of North America and China, the change in aerosol mass due to a 25% change in sulfur emissions is only 5-10%. This implies that in the polluted regions that are most interesting when discussing anthropogenic perturbations to the atmospheric aerosol system, nitrate aerosol needs to be accounted for when assessing the results of declining sulfur emissions (Metzger et al., submitted manuscript, 1998).

Aerosol nitrate concentrations change nearly linearly with changes in nitric acid concentrations, but the concentrations of other aerosol components are practically unchanged. Changes in ammonia emissions affect ammonium concentrations by 15% in the case of an increase and by 20% in the case of a decrease. Nitrate concentrations are affected by changes in ammonia emissions even more strongly than ammonium concentrations are, but sulfate concentrations and aerosol water content are nearly unchanged. Since sulfate and water constitute over 90% of aerosol mass, even 25% changes in nitric acid concentrations or ammonia emissions have little effect on total aerosol mass, since they have little effect on these two important components.

5. Conclusions

The global tropospheric sulfur and ammonia cycles, including emissions, chemistry, and wet and dry deposition, have been simulated together online in the GISS GCM II-prime. The local ammonium, nitrate, and water present in the aerosol at equilibrium for the conditions of temperature and relative humidity in each GCM grid cell have been calculated over a typical year. The output of a photochemical CTM has been used to specify the total amount of nitric acid available as a function of location and month. Concentrations of ammonia, ammonium, and nitrate simulated by the GCM have been compared with long-term surface observations made in North America and Europe, as well as to short-term observations in other regions and at higher altitudes.

The two factors that most strongly influence simulated ammonium concentrations are ammonia emissions and sulfate concentrations. Ammonium concentrations were high in most areas with high sulfate concentrations because these areas typically also have high ammonia emissions. Simulated ammonium concentrations were generally within a factor of 2 of annual average observed values. Ammonium concentrations were sometimes overestimated when associated with formation of nitrate aerosol. This seems to be the case in Europe, where the greatest tendency to overestimate ammonium concentrations occurred, as well as at some locations in North America.

Gas phase NH_3 concentrations are high in areas with high ammonia emissions, particularly if little sulfate is present. Ammonia concentrations are found to be highest globally in India. High ammonia concentrations are found almost exclusively within the boundary layer and decrease rapidly with altitude. Although our lowest model layer is only half as thick as that of DC94, our boundary layer resolution is still relatively coarse. This complicates comparison between model-generated surface layer concentrations and ground observations. It also introduces uncertainty into the calculated vertical transport of species in the boundary layer where the concentrations are largest, especially gas phase ammonia, which has the strongest vertical gradient. Simulated NH_3 concentrations did not compare as well with observations as did NH_4^+ concentrations. The ammonia concentration predicted by the model was within a factor of 2 of the observed value at just under half of the sites considered here. Much of the difficulty in comparing predicted ammonia concentrations with observations stems from its short lifetime, which implies that strong concentration gradients exist on spatial scales that the GCM cannot resolve.

It is estimated that about half of the 53.6 Tg N yr^{-1} of ammonia emissions is taken up by the aerosol phase to form ammonium. Ammonium has a longer lifetime, about 4 days, than ammonia, which has a lifetime of just 1 day. Three quarters of ammonia deposition occurs via dry processes, while wet deposition removes a similar fraction of ammonium from the atmosphere. Although the concentrations of ammonia and ammonium are similar in the model surface layer, the total tropospheric burden of ammonium, 0.30 Tg N, is about twice that of ammonia, 0.14 Tg N.

Substantial amounts of nitrate formation occur in polluted continental areas, especially during winter. In these areas, nitrate formation depends on the availability of ammonia in excess of that needed to neutralize sulfate. Nitrate and associated ammonium and water account for as much of the total aerosol mass as sulfate in midwestern North America as well as in a broad region of Europe and western Asia. Comparison with observations shows, however, that these predicted nitrate concentrations are high. On a global basis, the contribution of nitrate, with associated ammonium and water, to total aerosol mass is much smaller, only 11%. In marine areas, simulated nitrate concentrations are low in comparison to observations because uptake of nitric acid by sea salt is neglected in this work. In cold areas, such as in polar regions and the upper troposphere, nitrate aerosol can form in the absence of free ammonia because of its high solubility in water at lower temperatures.

Aerosol water content was generally highest in areas with high sulfate concentrations, although the effects of relative humidity and nitrate can also be seen. Because of these two factors, the amount of aerosol water uptake per mole of sulfate varied by 2 orders of magnitude. An accurate assessment of aerosol composition and water content is essential for a rigorous determination of the spatial distribution of aerosol radiative forcing.

The total global aerosol burden, including sulfate, nitrate, ammonium, and water, was estimated to be 7.5 Tg. Water constitutes, by itself, two thirds of the total aerosol mass, while the sulfate ion accounts for about 28%. The contributions of ammonium and nitrate to the overall burden were much lower, 5% and 1.7%, respectively. Several sensitivity runs were performed in which ammonia emissions, sulfur emissions, and nitric acid concentrations were each increased or decreased by 25% to evaluate how aerosol

formation responds to changes in its precursors. Changes in sulfur emissions have by far the largest impact on the global aerosol burden, with a 21% increase and 22% decrease, corresponding to a 25% increase and decrease in emissions, respectively. The effect of changing sulfur emissions on the global aerosol burden is very close to, but not quite, linear, because in polluted midlatitude regions, opposing changes in nitrate concentrations partly compensate for changes in sulfate levels. Nitrate therefore needs to be taken into account when calculating the total aerosol mass in anthropogenically influenced areas, or when predicting how aerosol mass will respond to changes in sulfate concentrations in these areas. Changes in HNO_3 concentrations have an effect on the nitrate burden, and changes in NH_3 emissions influence both the nitrate and ammonium burdens, but have little effect on total aerosol mass, which is dominated by water and sulfate.

The results of this study suggest several avenues for improvement and future research. First, the ammonia emissions inventory and nitric acid concentration fields need improvement to bring the amount of ammonium nitrate formation in the model into better agreement with the limited available observations. For example, both ammonia and ammonium tend to be too high in the simulation compared with EMEFS observations, indicating that the GEIA ammonia emissions inventory may simply be too high. Since formation of nitrate aerosol is sensitive to the availability of free ammonia and to the amount of total nitric acid present, observations of nitrate concentrations could provide a useful constraint on ammonia emissions and photochemical models. In particular, the correlation between high winter nitrate concentrations and high ammonia concentrations suggests that ammonia emissions may be too high during that time of year. Second, more long-term observations, especially outside North America and Europe and of ammonia and nitrate, are required to better evaluate global simulations. A greater density of observational sites can help eliminate the problem of subgrid variability that arises when comparing output from such a large-scale model with observations because of the short lifetimes of aerosol ions and ammonia. Another improvement that could be made would be to simulate nitric acid in a way that is more consistent with the rest of the aerosol simulation. Ideally, the simulation of the sulfur and ammonia cycles presented here would be fully coupled to a photochemical model. Another possibility would be to use production rates of nitric acid taken from a photochemical CTM as input to this model. In that case, gas phase nitric acid and particulate nitrate would be included in the GCM as tracers, and their transport, deposition, and chemical destruction (i.e., photolysis of gas phase nitric acid) would be explicitly included in the GCM simulation. This would allow the wet and dry deposition schemes to take into account the gas-aerosol partitioning of total nitrate and the GCM to calculate a total nitrate budget rather than just the burden of particulate nitrate. Finally, a natural extension of the present work is to evaluate the effect of variable aerosol composition and water uptake on global and regional radiative forcing.

Acknowledgments. This work has been supported by a graduate fellowship from the Fannie and John Hertz Foundation as well as by the National Aeronautics and Space Administration Earth Observing System Interdisciplinary Science program (NASA EOS-IDS). We would also like to acknowledge the Center for Advanced Computing Research at Caltech for computational resources, Loretta Mickley and fellow researchers at Harvard University for nitric acid concentration fields from the Harvard CTM, and Lex Bouwman at the National Institute of Public Health and the Environment in Bilthoven, Netherlands, for providing us with the GEIA ammonia emissions inventory in advance of publication. The EMEFS data utilized in this study were collected and prepared under the sponsorship of the Electric Power Research Institute. EMEP data were obtained from the Norwegian Institute for Air Research. We also thank two anonymous reviewers for helpful comments and constructive criticism.

References

Andreae, M. O., H. Berresheim, T. W. Andreae, M. A. Kritz, T. S. Bates, and J. T. Merrill, Vertical distribution of dimethyl sulfide, sulfur dioxide, aerosol ions, and radon over the northeast Pacific Ocean, *J. Atmos. Chem., 6*, 149-173, 1988.

Ansari, A. S., and S. N. Pandis, Response of inorganic PM to precursor concentrations, *Environ. Sci. Technol. , 32*, 2706-2714, 1998.

Asman, W. A. H., and H. A. van Jaarsveld, A variable-resolution transport model applied for NH_x in Europe, *Atmos. Environ., Part A, 26*, 445-464, 1992.

Bassett, M. E., and J. H. Seinfeld, Atmospheric equilibrium model of sulfate and nitrate aerosol, *Atmos. Environ., 17*, 2237-2252, 1983.

Bassett, M. E., and J. H. Seinfeld, Atmospheric equilibrium model of sulfate and nitrate aerosol, II, Particle size analysis, *Atmos. Environ., 18*, 1163-1170, 1984.

Berresheim, H., M. O. Andreae, G. P. Ayers, R. W. Gillett, J. T. Merrill, V. J. Davis, and W. L. Chameides, Airborne measurements of dimethyl sulfide, sulfur dioxide, and aerosol ions over the Southern Ocean south of Australia, *J. Atmos. Chem., 10*, 341-370, 1990.

Berresheim, H., M. O. Andreae, R. L. Iverson, and S. M. Li, Seasonal variations of dimethylsulfide emissions and atmospheric sulfur and nitrogen species over the western North Atlantic Ocean, *Tellus, Ser.B, 43*, 353-372, 1991.

Boucher, O., GCM estimate of the indirect aerosol forcing using satellite-retrieved cloud droplet effective radii, *J. Clim., 8*, 1403-1409, 1995.

Boucher, O., and T. L. Anderson, General circulation model assessment of the sensitivity of direct climate forcing by anthropogenic sulfate aerosols to aerosol size and chemistry, *J. Geophys. Res., 100*, 26,117-26,134, 1995.

Boucher, O., and U. Lohmann, The sulfate-CCN-cloud albedo effect, *Tellus, Ser. B, 47*, 281-300, 1995.

Bouwman, A. F., D. S. Lee, W. A. H. Asman, F. J. Dentener, K. W. Van Der Hoek, and J. G. J. Olivier, A global high-resolution emission inventory for ammonia, Global Biogeochem. *Cycles, 11*, 561-587, 1997.

Cadle, S. H., J. M. Dasch, and P. A. Mulawa, Atmospheric concentrations and the deposition velocity to snow of nitric acid, sulfur dioxide and various particulate species, *Atmos. Environ., 19*, 1819-1827, 1985.

Charlson, R. J., J. Langner, H. Rodhe, C. B. Leovy, and S. G. Warren, Perturbation of the northern hemisphere radiative balance by backscattering from anthropogenic sulfate aerosols, *Tellus, Ser. AB, 43*, 152-163, 1991.

Chin, M., D. J. Jacob, G. M. Gardner, M. S. Foreman-Fowler, and P. A. Spiro, A global three-dimensional model of tropospheric sulfate, *J. Geophys. Res., 101*, 18,667-18,690, 1996.

Chuang, C. C., J. E. Penner, K. E. Taylor, A. S. Grossman, and J. J. Walton, An assessment of the radiative effects of anthropogenic sulfate, *J. Geophys. Res., 102*, 3761-3778, 1997.

Church, T. M. , J. M. Tramontano, D. M. Whelpdale, M. O. Andreae, J. N. Galloway, W. C. Keene, A. H. Knap, and J. Tokos Jr., Atmospheric and precipitation chemistry over the North Atlantic Ocean: Shipboard results, April-May 1984, *J. Geophys. Res., 96*, 18,705-18,725, 1991.

Clairac, B., R. Delmas, B. Cros, H. Cachier, P. Buat-Ménard, and J. Servant, Formation and chemical composition of atmospheric aerosols in an equatorial forest area, *J. Atmos. Chem., 6*, 301-322, 1988.

Clarke, A. D., and J. N. Porter, Pacific marine aerosol, 2, Equatorial gradients in chlorophyll, ammonium, and excess sulfate during SAGA 3, *J. Geophys. Res., 98*, 16,997-17,010, 1993.

Clegg, S. L., K. S. Pitzer, and P. Brimblecombe, Thermodynamics of multicomponent, miscible, ionic solutions. II. Mixture including unsymmetrical electrolytes, *J. Phys. Chem., 96*, 9470-9479, 1992.

(Additions and corrections, *J. Phys. Chem., 98*, 1368, 1994; *J. Phys. Chem., 99*, 6755, 1995.)

Clegg, S. L., P. Brimblecombe, and A. S. Wexler, A thermodynamic model of the system H^+-NH_4^+-Na^+-SO_4^{2-}-NO_3^--Cl^--H_2O at 298.15 K, *J. Phys. Chem., 102*, 2155-2171, 1998a.

Clegg, S. L., P. Brimblecombe, and A. S. Wexler, A thermodynamic model of the system H^+-NH_4^+-Na^+-SO_4^{2-}-NO_3^--Cl^--H_2O at tropospheric temperatures, *J. Phys. Chem., 102*, 2137-2154, 1998b.

Coffman, D. J., and D. A. Hegg, A preliminary study of the effect of ammonia on particle nucleation in the marine boundary layer, *J. Geophys. Res., 100*, 7147-7160, 1995.

Covert, D. S., North Pacific marine background aerosol: Average ammonium to sulfate molar ratio equals 1, *J. Geophys. Res., 93*, 8455-8458, 1988.

Del Genio, A. D., and M.-S. Yao, Efficient cumulus parameterization for long-term climate studies: The GISS scheme, in *The Representation of Cumulus Convection in Numerical Models* Monogr. 46, edited by K. A. Emanuel and D. J. Raymond, pp. 181-184, Am. Meteorol. Soc., Boston, Mass., 1993.

Del Genio, A. D., M.-S. Yao, W. Kovari, and K. K.-W. Lo, A prognostic cloud water parameterization for global climate models, *J. Clim., 9*, 270-304, 1996.

DeMore, W. B., S. P. Sander, D. M. Golden, R. F. Hampson, M. J. Kurylo, C. J. Howard, A. R. Ravishankara, C. E. Kolb, and M. J. Molina, Chemical kinetics and photochemical data for use in stratospheric modeling: Evaluation number 12, JPL Publ., 97-4, 1997.

Dentener, F. J., and P. Crutzen, A three-dimensional model of the global ammonia cycle, *J. Atmos. Chem., 19*, 331-369, 1994.

Erickson, D. J., J. J. Walton, S. J. Ghan, and J. E. Penner, Three-dimensional modeling of the global atmospheric sulfur cycle: A first step, *Atmos. Environ., Part A, 25*, 2513-2520, 1991.

Erickson, D. J., R. J. Oglesby, and S. Marshall, Climate response to indirect anthropogenic sulfate forcing, *Geophys. Res. Lett., 22*, 2017-2020, 1995.

Feichter, J., E. Kjellstrom, H. Rodhe, F. Dentener, J. Lelieveld, and G.-J. Roelofs, Simulation of the tropospheric sulfur cycle in a global climate model, *Atmos. Environ., 30*, 1693-1707, 1996.

Feichter, J., U. Lohmann, and I. Schult, The atmospheric sulfur cycle in ECHAM-4 and its impact on the shortwave radiation, *Clim. Dyn., 13*, 235-246, 1997.

Fekete, K. E., and L. Gyenes, Regional-scale transport model for ammonia and ammonium, *Atmos. Environ. Part A, 27*, 1099-1104, 1993.

Galloway, J. N., Acid deposition: Perspectives in time and space, *Water, Air and Soil Pollution, 85*, 15-24, 1995.

Galperin, M. V., and M. A. Sofiev, The long-range transport of ammonia and ammonium in the Northern Hemisphere, *Atmos. Environ., 32*, 373-380, 1998.

Gras, J. L., Ammonia and ammonium concentrations in the Antarctic atmosphere, *Atmos. Environ., 17*, 815-818, 1983.

Gregory, G. L., et al., Air chemistry over the tropical forest of Guyana, *J. Geophys. Res., 91*, 8603-8612, 1986.

Hansen, J., G. Russell, D. Rind, P. Stone, A. Lacis, S. Lebedeff, R. Ruedy, and L. Travis, Efficient three-dimensional global models for climate studies: Models I and II, Mon. *Weather Rev., 111*, 609-662, 1983.

Hanssen, J. E., U. Pedersen, J. Schlaug, H. Dovland, J. M. Pacyna, A. Semb, and J. E. Skjelmoen, Summary report from the Chemical Co-ordinating Centre for the fourth phase of EMEP, *EMEP/CCC Rep. 2/90*, Norw. Inst. for Air Res., Lillestrom, 1990.

Harrison, R. M., and C. A. Pio, Size-differentiated composition of inorganic atmospheric aerosols of both marine and polluted continental origin, *Atmos. Environ., 17*, 1733-1738, 1983.

Hartke, G. J., and D. Rind, Improved surface and boundary layer models for the Goddard Institute for Space Studies general circulation model, *J. Geophys. Res., 102*, 16,407-16,422, 1997.

Haywood, J. M., and K. P. Shine, The effect of anthropogenic sulfate and soot aerosol on the clear sky planetary radiation budget, *Geophys. Res. Lett., 22*, 603-606, 1995.

Haywood, J. M., and V. Ramaswamy, Global sensitivity studies of the direct radiative forcing due to anthropogenic sulfate and black carbon aerosols, *J. Geophys. Res., 103*, 6043-6058, 1998.

Haywood, J. M., D. L. Roberts, A. Slingo, J. M. Edwards, and K. P. Shine, General circulation model calculations of the direct radiative forcing by anthropogenic sulfate and fossil-fuel soot aerosol, *J. Clim., 10*, 1562-1577, 1997.

Hjellbrekke, A.-G., and J. E. Hanssen, Data report 1996, 1, Annual summaries., *EMEP/CCC Rep. 1/98*, 85 pp., Norw. Inst. for Air Res., Lillestrom, 1998.

Horowitz, L. W., J. Liang, G. M. Gardner, and D. J. Jacob, Export of reactive nitrogen from North America during summertime: Sensitivity to hydrocarbon chemistry, *J. Geophys. Res., 103*, 13,451-13,476, 1998.

Hov, Ø., B. A. Hjøllo, and A. Eliassen, Transport distance of ammonia and ammonium in northern Europe, 1, Model description, J. *Geophys. Res., 99*, 18,735-18,748, 1994.

Huebert, B. J., Wang. Ming-Xing, and Lü Wei-Xiu, Atmospheric nitrate, sulfate, ammonium, and calcium concentrations in China, *Tellus, Ser. B, 40*, 260-269, 1988.

Huebert, B. J., L. Zhuang, S. Howell, K. Noone, and B. Noone, Sulfate, nitrate, methanesulfonate, chloride, ammonium, and sodium measurements from ship, island, and aircraft during the Atlantic Stratocumulus Transition Experiment/Marine Aerosol Gas Exchange, *J. Geophys. Res., 101*, 4413-4423, 1996.

Intergovernmental Panel on Climate Change (IPCC), *Climate Change 1995*, edited by J. T. Houghton et al., Cambridge Univ. Press, New York, 1996.

Iversen T., N.E. Halvorsen, S. Mylona, and H. Sandnes, Calculated budgets for airborne acidifying components in Europe, 1985, 1987, 1988, 1989 and 1990, *EMEP/MSW-Rep. 1-91*, Norw. Inst. for Air Res., Lillestrom, 1991.

Jacob, D. J. , J. W. Munger, J. M. Waldman, and M. R. Hoffmann, The H_2SO_4-HNO_3-NH_3 sytem at high humidities and in fogs, 1, Spatial and temporal patterns in the San Joaquin Valley of California, *J. Geophys. Res., 91*, 1073-1088, 1986.

Jacob, D. J., et al., Simulation of summertime ozone over North America, *J. Geophys. Res., 98*, 14,797-14,816, 1993.

Jacobson, M. Z., A. Tabazadeh, and R. P. Turco, Simulating equilibrium within aerosols and nonequilibrium between gases and aerosols, *J. Geophys. Res., 101*, 9079-9091, 1996.

John, W., S. M. Wall, J. L. Ondo, and W. Winklmayr, Modes in the size distribution of atmospheric inorganic aerosol, *Atmos. Environ., Part A, 24*, 2349-2359, 1990.

Jones, A., D. L. Roberts, and A. Slingo, A climate model study of indirect radiative forcing by anthropogenic sulphate aerosols, *Nature, 370*, 450-453, 1994.

Kasibhatla, P., W. L. Chameides, and J. St. John, A three-dimensional global model investigation of seasonal variations in the atmospheric burden of anthropogenic aerosols, *J. Geophys. Res., 102*, 3737-3759, 1997.

Keeler, G. J., J. D. Spengler, and R. A. Castillo, Acid aerosol measurements at a suburban Connecticut site, *Atmos. Environ., Part A, 25*, 681-690, 1991.

Khemani, L. T., G. A. Momin, M. S. Naik, R. Vijayakumar, and B. V. Ramana Murty, Chemical composition and size distribution of atmospheric aerosols over the Deccan Plateau, India, *Tellus, 34*, 151-158, 1982.

Kiehl, J. T., and B. P. Briegleb, The relative roles of sulfate aerosols and greenhouse gases in climate forcing, *Science, 260*, 311-314, 1993.

Kim, Y. P., and J. H. Seinfeld, Atmospheric gas-aerosol equilibrium, III, Thermodynamics of crustal elements Ca^{2+}, K^+, and Mg^{2+}, *Aerosol Sci. Technol., 22*, 93-110, 1995.

Kim, Y. P., J. H. Seinfeld, and P. Saxena, Atmospheric gas-aerosol equilibrium, I, Thermodynamic model, *Aerosol Sci. Technol., 19*, 157-181, 1993a.

Kim, Y. P., J. H. Seinfeld, and P. Saxena, Atmospheric gas-aerosol equilibrium, II, Analysis of common approximations and activity coefficient calculation methods, *Aerosol Sci. Technol., 19*, 182-198, 1993b.

Kjellstrom, E., A three-dimensional global model study of carbonyl sulfide in the troposphere and the lower stratosphere, *J. Atmos. Chem., 29*, 151-177, 1998.

Kulmala, M., A. Laaksonen, P. Korhonen, T. Vesala, and T. Ahonen, The effect of atmospheric nitric acid vapor on cloud condensation nucleus activation, *J. Geophys. Res., 98*, 22,949-22,958, 1993.

Kulshrestha, U. C., A. Saxena, N. Kumar, K. M. Kumari, and S. S. Srivastava, Chemical composition and association of size-differentiated aerosols at a suburban site in a semi-arid tract of India, *J. Atmos. Chem., 29*, 109-118, 1998.

Langford, A. O., F. C. Fehsenfeld, J. Zachariassen, and D. S. Schimel, Gaseous ammonia fluxes and background concentrations in terrestrial

ecosystems of the United States, Global Biogeochem. *Cycles, 6*, 459-483, 1992.

Langner, J. and H. Rodhe, A global three-dimensional model of the tropospheric sulfur cycle, *J. Atmos. Chem., 13*, 225-263, 1991.

Lelieveld, J., G.-J. Roelofs, L. Ganzeveld, J. Feichter, and H. Rodhe, Terrestrial sources and distribution of atmospheric sulphur, *Philos. Trans. R. Soc. London, 352*, 149-158, 1997.

Lenhard, U., and G. Gravenhorst, Evaluation of ammonia fluxes into the free atmosphere over western Germany, *Tellus, 32*, 48-55, 1980.

Lindberg, S. E., M. Bredemeier, D. A. Schaefer, and L. Qi, Atmospheric concentrations and deposition of nitrogen and major ions in conifer forests in the United States and Federal Republic of Germany, *Atmos. Environ., Part A, 24*, 2207-2220, 1990.

Lohmann, U., and J. Feichter, Impact of sulfate aerosols on albedo and lifetime of clouds: A sensitivity study with the ECHAM4 GCM, *J. Geophys. Res., 102*, 13,685-13,700, 1997.

McNaughton, D. J., and R. J. Vet, Eulerian model evaluation field study (EMEFS): A summary of surface network measurements and data quality, *Atmos. Environ., 30*, 227-238, 1996.

Meng, Z., and J. H. Seinfeld, Time scales to achieve atmospheric gas-aerosol equilibrium for volatile species, *Atmos. Environ., 30*, 2889-2900, 1996.

Meng, Z., J. H. Seinfeld, P. Saxena, and Y. P. Kim, Atmospheric gas-aerosol equilibrium, IV, Thermodynamics of carbonates, *Aerosol Sci. Technol., 23*, 131-154, 1995.

Mészáros, E., and L. Horváth, Concentration and dry deposition of atmospheric sulfur and nitrogen compounds in Hungary, *Atmos. Environ., 18*, 1725-1730, 1984.

Mészáros, E., T. Barcza, A. Gelencsér, J. Hlavay, Gy. Kiss, Z. Krivácsy, A. Molnár, and K. Polyák, Size distributions of inorganic and organic species in the atmospheric aerosol in Hungary, *J. Aerosol Sci., 28*, 1163-1175, 1997.

Metcalfe, S. E., J. D. Whyatt, and R. G. Derwent, Multi-pollutant modelling and the critical loads approach for nitrogen, *Atmos. Environ., 32*, 401-408, 1998.

Mitchell, J. F. B., and T. C. Johns, On modification of global warming by sulfate aerosols, *J. Clim., 10*, 245-267, 1997.

Mitchell, J. F. B., T. C. Johns, J. M. Gregory, and S. F. B. Tett, Climate response to increasing levels of greenhouse gases and sulphate aerosols, *Nature, 376*, 501-504, 1995a.

Mitchell, J. F. B., R. A. Davis, W. J. Ingram, and C. A. Senior, On surface temperature, greenhouse gases, and aerosols: Models and observations, *J. Clim., 8*, 2364-2386, 1995b.

National Research Council, *A Plan for a Research Program on Aerosol Radiative Forcing and Climate Change*, edited by J. H. Seinfeld et al., Nat. Acad. Press, Washington, D.C., 1996.

Nenes, A., C. Pilinis, and S. N. Pandis, Isorropia: A new thermodynamic equilibrium model for multiphase multicomponent inorganic aerosols, *Aquat. Geochem., 4*, 123-152, 1998.

Ohta, S., and T. Okita, A chemical characterization of atmospheric aerosol in Sapporo, *Atmos. Environ., Part A, 24*, 815-822, 1990.

Ohta, S., N. Murao, and V. N. Makarov, *Geochemical study of atmospheric aerosols in Yakutsk*, paper presented at Permafrost Environment, Hokkaido Univ., Sapporo, Japan, 1992.

Oort, A. H., *Global atmospheric circulation statistics*, 1958-1973, NOAA Prof. Pap. 14, U.S. Gov. Print. Off., Washington, D. C., 1983.

Pakkanen, T. A., et al., Nordic intercomparison for measurement of major atmospheric nitrogen species, *J. Aerosol Sci., 30*, 247-263, 1999.

Parungo, F. P., C. T. Nagamoto, J. Rosinski, and P. L. Haagenson, A study of marine aerosols over the Pacific Ocean, *J. Atmos. Chem., 4*, 199-226, 1986.

Penner, J. E., C. S. Atherton, and T. E. Graedel, *Global emissions and models of photochemically active compounds, in Global Atmospheric-Biospheric Chemistry*, edited by R. G. Prinn, pp. 223-247, Plenum, New York, 1994.

Pham, M., J.-F. Muller, G. P. Brasseur, C. Granier, and G. Megie, A three-dimensional study of the tropospheric sulfur cycle, *J. Geophys. Res., 100*, 26,061-26,092, 1995.

Pierson, W. R., W. W. Brachaczek, R. A. Gorse Jr., S. M. Japar, and J. M. Norbeck, Atmospheric acidity measurements on Allegheny Mountain and the origins of ambient acidity in the northeastern United States, *Atmos. Environ., 23*, 431-459, 1989.

Pilinis, C., and J. H. Seinfeld, Continued development of a general equilibrium model for inorganic multicomponent atmospheric aerosols, *Atmos. Environ., 32*, 2453-2466, 1987.

Quinn, P. K., R. J. Charlson, and W. H. Zoller, Ammonia, the dominant base in the remote marine troposphere: a review, *Tellus, Ser. B, 39*, 413-425, 1987.

Quinn, P. K., T. S. Bates, J. E. Johnson, D. S. Covert, and R. J. Charlson, Interactions between the sulfur and reduced nitrogen cycles over the central Pacific Ocean, *J. Geophys. Res., 95*, 16,405-16,416, 1990.

Rind, D., and J. Lerner, The use of on-line tracers as a diagnostic tool in general circulation model development, 1, Horizontal and vertical transport in the troposphere, *J. Geophys. Res., 101*, 12,667-12,683, 1996.

Roelofs, G.-J., J., Lelieveld, and L. Ganzeveld, Simulation of global sulfate distribution and the influence on effective cloud drop radii with a coupled photochemistry-sulfur cycle model, *Tellus, Ser. B, 50*, 224-242, 1998.

Saxena, P., C. Seigneur, A. B. Hudischewskyj, and J. H. Seinfeld, A comparative study of equilibrium approaches to the chemical characterizations of secondary aerosols, *Atmos. Environ., 20*, 1471-1484, 1986.

Schlesinger, W. H., and A. E. Hartley, A global budget for atmospheric NH_3, Biogeochemistry, 15, 191-211, 1992.

Seinfeld, J. H., and S. N. Pandis, *Atmospheric Chemistry and Physics*, John Wiley, New York, 1998.

Singles, R., M. A. Sutton, and K. J. Weston, A multi-layer model to describe the atmospheric transport and deposition of ammonia in Great Britain, *Atmos. Environ., 32*, 393-399, 1998.

Suh, H. H., G. A. Allen, B. Aurian-Blajeni, P. Koutrakis, and R. M. Burton, Field method comparison for the characterization of acid aerosols and gases, *Atmos. Environ., 28*, 2981-2989, 1994.

Syri, S., M. Johansson, and L. Kangas, Application of nitrogen transfer matrices for integrated assessment, *Atmos. Environ., 32*, 409-413, 1998.

Tabazadeh, A., M. Z. Jacobson, H. B. Singh, O. B. Toon, J. S. Lin, R. B. Chatfield, A. N. Thakur, R. W. Talbot, and J. E. Dibb, Nitric acid scavenging by mineral and biomass burning aerosols, *Geophys. Res. Lett., 25*, 4185-4188, 1998.

Talbot, R. W., R. C. Harriss, E. V. Browell, G. L. Gregory, D. I. Sebacher, and S. M. Beck, Distribution and geochemistry of aerosols in the tropical North Atlantic troposphere: relationship to Saharan dust, *J. Geophys. Res., 91*, 5173-5182, 1986.

Talbot, R. W., M. O. Andreae, T. W. Andreae, and R. C. Harriss, Regional aerosol chemistry of the Amazon Basin during the dry season, *J. Geophys. Res., 93*, 1499-1508, 1988.

Talbot, R. W., M. O. Andreae, H. Berresheim, P. Artaxo, M. Garstang, R. C. Harriss, K. M. Beecher, and S. M. Li, Aerosol chemistry during the wet season in central Amazonia: The influence of long-range transport, *J. Geophys. Res., 95*, 16,955-16,969, 1990.

Talbot, R. W., A. S. Vijgen, and R. C. Harriss, Soluble species in the Arctic summer troposphere: Acidic gases, aerosols, and precipitation, *J. Geophys. Res., 97*, 16,531-16,543, 1992.

van Dorland, R., F. J. Dentener, and J. Lelieveld, Radiative forcing due to tropospheric ozone and sulfate aerosols, *J. Geophys. Res., 102*, 28,079-28,100, 1997.

Wang, Y., D. J. Jacob, and J. A. Logan, Global simulation of tropospheric O_3-NO_x-hydrocarbon chemistry, 1, Model formulation, *J. Geophys. Res., 103*, 10,713-10,725, 1998a.

Wang, Y., D. J. Jacob, and J. A. Logan, Global simulation of tropospheric O_3-NO_x-hydrocarbon chemistry, 2, Model evaluation and global ozone budget, *J. Geophys. Res., 103*, 10,727-10,755, 1998b.

Warneck, P., Nitrogen compounds in the troposphere, in Chemistry of the Natural Atmosphere, Academic, San Diego, Calif., 1988.

Wesely, M. L., Parameterization of surface resistances to gaseous dry deposition in regional-scale numerical models, *Atmos. Environ., 23*, 1293-1304, 1989.

Wesely, M. L., and B. B. Hicks, Some factors that affect the deposition rates of sulfur dioxide and similar gases on vegetation, *J. Air Pollut. Contr. Assoc., 27*, 1110-1116, 1977.

West, J. J., C. Pilinis, A. Nenes, and S. N. Pandis, Marginal direct climate forcing by atmospheric aerosols, *Atmos. Environ., 32*, 2531-2542, 1998.

Wexler, A. S., and J. H. Seinfeld, The distribution of ammonium salts among a size and composition dispersed aerosol, *Atmos. Environ., Part A, 24*, 1231-1246, 1990.

Wexler, A. S., and J. H. Seinfeld, Second-generation inorganic aerosol model, *Atmos. Environ., Part A, 25*, 2731-2748, 1991.

Whelpdale, D. M., W. C. Keene, A. D. A. Hansen, and J. Boatman,

Aircraft measurements of sulfur, nitrogen, and carbon species during WATOX-86, Global Biogeochem. *Cycles, 1,* 357-368, 1987.

Yoshizumi, K., and K. Asakuno, Characterization of atmospheric aerosols in Chichi of the Ogasawara (Bonin) Islands, *Atmos. Environ., 20,* 151-155, 1986.

P. Adams and J. H. Seinfeld, Department of Chemical Engineering, California Institute of Technology, 1200 East California Boulevard, Pasadena, CA 91125. (petera@cco.caltech.edu; seinfeld@cco.caltech.edu)

D. M. Koch, National Aeronautics and Space Administration Goddard Institute for Space Studies, 2880 Broadway, New York, NY 10025. (koch@hess.geology.yale.edu)

(Received November 13, 1998; revised January 27, 1999; accepted February 8, 1999.)